ICEQUAKES AND ICE MOTION: A TIME-SERIES ANALYSIS OF THE DYNAMICS OF THE BERING GLACIER, ALASKA

A

THESIS

Presented to the Faculty

of the University of Alaska Fairbanks

in Partial Fulfillment of the Requirements

for the Degree of

MASTER OF SCIENCE

By

Laura E. LeBlanc, B.S.

Fairbanks, AK

December 2009

ABSTRACT

We have acquired a year-long GPS record and a 16-month seismic data set from an array of co-located seismic and GPS stations established on Bering Glacier, Alaska in spring 2007. A strong correlation exists between icequake occurrence and ice motion. The GPS motion record gives a mean annual horizontal velocity of 1.2 m d^{-1} and shows evidence of a spring speed-up, diurnal velocity fluctuations in summertime with peaks of up to 4 m d^{-1}, a transient peak of 8 m d^{-1} associated with a major rainstorm, and winter quiescence. Over 1.5 million icequakes were detected, with rates of up to 600 events per hour. The seismic record shows an onset of high activity associated with spring speed up, followed by a shift into diurnal behavior by mid-summer. The seismic and motion records may reflect several reorganizations of the glacial hydraulic system that occurred in the late spring, in the fall, and in the late winter. Detected icequakes were organized into groups of similar waveforms to better investigate repeating events and associated source mechanisms. We propose several seismic source mechanisms to explain the time-series relationship between icequakes and ice motion including ice fracture, hydraulic transients, and basal recoupling.

TABLE OF CONTENTS

LIST OF FIGURES

Page

LIST OF TABLES

Page

LIST OF APPENDICES

Page

ACKNOWLEDGEMENTS

Thanks to the National Science Foundation Geophysics Program (EAR-0607872) for their generous support of this project. Equipment for the field campaign was provided by PASSCAL (seismic) and UNAVCO (GPS). Thanks to the folks at CH2MHill (formerly VECO) Polar Resources for their help and availability in outfitting us for our field campaign. Paul Claus, of Ultima Thule Outfitters, and Jan Gunderson, of ERA Helicopters, provided high caliber transportation to and support for our field sites. Kudos to Ryan Cross, who went above-and-beyond in his participation during our remote site installations. Thanks also to Julie Elliott and David Podrasky for their voluntary efforts during summer site maintenance. Jeff Freymueller (GI Geodesy group) lent guidance in processing the GPS data using GIPSY. Natasha Ruppert (GI Seismology) provided valuable help with the initial seismic data processing. Thanks to Andy Aschwanden and Sam Herreid for their thoughtful reviews. Thanks to my advisor, Chris Larsen, for his patience, support, and helpful advice. Thanks to my committee (Doug Christensen, Roman Motyka, Martin Truffer, and Mike West) for their time, expertise, and valuable edits. Thanks to my fellow students and colleagues of the 'Glaciers Lab' for the humor, support, and good coffee that gets us through. Thanks to my family for their unending support and encouragement. And lastly, thanks to the best four-legged study mate who remained loyal even after too many late night hours at the office.

1. INTRODUCTION

The dynamics of a glacier system are constantly changing in response to seasonal and diurnal variations in water input and storage. This is evidenced by daily to seasonal variations in surface velocities. A glacier moves by three processes: plastic deformation of the ice, sliding over the bed, and deformation of the bed (Paterson, 1994). Basal sliding is the principal form of movement of most temperate glaciers. Sliding is promoted by both elevated water pressure and water storage at the bed. These processes increase the separation of the ice from the bed, which results in decreased basal traction and enhanced basal motion (Iken et al., 1983; Kamb et al., 1994; Paterson, 1994). Basal water pressure is determined by water supply hydraulic conductivity, and interconnectivity of subglacial cavities (Iken and Truffer, 1997). Fluctuations of water input can cause variations in sliding velocities, but those variations depend on the current state of the hydraulic system (Bartholomaus et al., 2008).

Many temperate glaciers exhibit summertime velocities that are highly variable and can be 20-100% greater than mean winter velocities (Willis, 1995). The transition during the beginning of the ablation season from slow to fast flow is often referred to as the "spring speed-up". The increase in velocity is attributed to an increase in basal motion caused by a rise in the melt-water flux to the basal hydraulic system (Röthlisberger and Lang, 1987). Diurnal fluctuations in surface velocity have been observed during summer months on numerous glaciers. On temperate glaciers, diurnal cycles are typically 150% to 500% of the background summertime velocity (Willis, 1995). These fluctuations are presumably the result of diurnal melt input. Increases in basal water pressure, and resultant increases in surface velocities, can also be caused by the release and transport of stored water from supraglacial, englacial, or basal sources to the bed (Fountain and Walder, 1998).

Icequakes are seismic events originating from within the glacier and can be caused by both changes in velocity and changes in the hydraulic network. We established an array of co-located GPS (Global Positioning System) and seismic stations on the Bering Glacier, AK to examine the relation between icequakes and ice motion. From this field campaign, we acquired a yearlong continuous GPS motion record (April 2007-2008) and a 16-month seismic data set (April 2007-July 2008).

We used these records of ice motion and icequakes to gain a better understanding of the seasonal and diurnal evolution of glacier dynamics. The correlation between icequake occurrence

and ice motion can reveal the timing of changes in the hydraulic system and stress regime that may not be evident in the motion record alone. The drainage system under a glacier is comprised of either a slow, nonarborescent network of conduits, cavities, and permeable till or a fast, arborescent network of connected channels (Fountain and Walder, 1998). A glacier bed may also host both systems, with transitional zones linking the two. The basal drainage system can switch from one configuration to the other in response to changing meltwater input. When and where these two systems exist determines the effects of water input on the basal velocities (Kessler and Anderson, 2004). Velocity variations result from changes in the amount of basal sliding or deformation of the basal till governed by fluctuations of the subglacial water pressure or water storage capacity (Kamb et al., 1994).

Past studies have used icequakes to improve understanding of ice fracture mechanisms (Deichmann et al., 2000; Walter et al., 2008) and calving (Qamar, 1988; O'Neel and Pfeffer, 2007; Amundson et al., 2008), as well as the conditions beneath Antarctic ice streams (Anandakrishnan and Bentley, 1993; Smith, 2006). However, there have been very few studies in which GPS motion and seismic data were concurrently acquired at the same location (Wiens et al., 2008; Walter et al., 2008), and none over such a long duration as our data set. We use a high-resolution motion record to provide better insight into icequake mechanisms and to produce a more robust understanding of the relation between ice motion, icequakes, and the evolving glacial hydraulic system.

We observed diurnal and seasonal trends in icequake occurrence and ice motion that suggest shifts in the basal hydraulic network. A spring speed-up coincided with high rates of icequake activity, which imply a change in basal hydraulics. By mid-summer, there was a strong diurnal signal present in both the velocity and the icequake occurrence, indicative of the development of a well-connected drainage system. Similar diurnal variations in motion and seismicity have been observed on Gornergletscher (Walter et al., 2008). A heavy fall rainstorm, which coincided with a distinct change in both velocity and icequake activity, likely caused a reorganization of the hydraulic network (Hubbard and Nienow, 1997; Bartholomaus et al., 2008). Small increases in velocity during the winter were echoed by comparatively large peaks in icequake occurrence, which suggest ongoing changes in the basal stress regime during winter quiescence.

2. FIELD SETTING

The Bering Glacier is a temperate lake-calving piedmont glacier that is part of the Bering-Bagley Icefield system located in South Central Alaska (Fig. 1). The Bering-Bagley system covers an area of 3630 km^2 with an accumulation area ratio (AAR) of 0.43 and an equilibrium line altitude (ELA) of approximately 1500 m (Beedle et al., 2008). The glacier is up to 1200 m thick (Conway et al., 2009). Bering is the largest glacier in the U.S. and, at 191 km long, is the longest glacier in North America (Molnia and Post, 1995). Bering is a coastal glacier that experiences a maritime climate. Annual accumulations of approximately 3 myr^{-1} water equivalent (w.e.) are measured at sea-level meteorological stations (Cordova and Yakutat stations, Western Regional Climate Center, www.raws.dri.edu) and annual precipitations of 5-13 myr^{-1} w.e. have been estimated for the Bering Glacier accumulation area (Daly et al., 1994). A portion of the glacier terminates in Vitus Lake, roughly 10 km from the Gulf of Alaska. Bering Glacier is also a surge-type glacier with a period of approximately 17 to 26 years, with renewed surges or secondary pulses sometimes occurring at shorter intervals (Molnia and Post, 1995) . The most recent documented surge was in 1993-95. As a surge-type glacier, it is possible that Bering is at least partially underlain by a layer of till (Harrison and Post, 2003).

In April 2007, we established a strain diamond of four co-located seismic/GPS stations (MILR, STLR, CRAK, SMEL), located roughly halfway between the equilibrium line and terminus where the glacier is about 10 km wide (Fig.1) and ~700 m thick (Conway et al., 2009). A fifth seismic station (BMG) was established at the center of the co-located stations with a 4-km aperture. A fifth GPS station (JNPR) was placed roughly 20 km up glacier from the lower stations, near where the Bagley narrows and turns to the Bering. A GPS base station was installed at the Bering Glacier Camp, on the shore of Vitus Lake, approximately 35 km from the strain diamond.

There is a large (several sq. km) surface depression in the vicinity of the lower stations (MILR, CRAK, STLR, BMG, SMEL), which is probably indicative of a bed depression under the glacier. In the late spring and early summer, a surface lake is present in this area. The ice in this region flows uphill out of the depression, likely over a rise in the bed. This uphill motion, unusual in most glaciers, would not be possible through ice deformation and must result from large amounts of basal sliding.

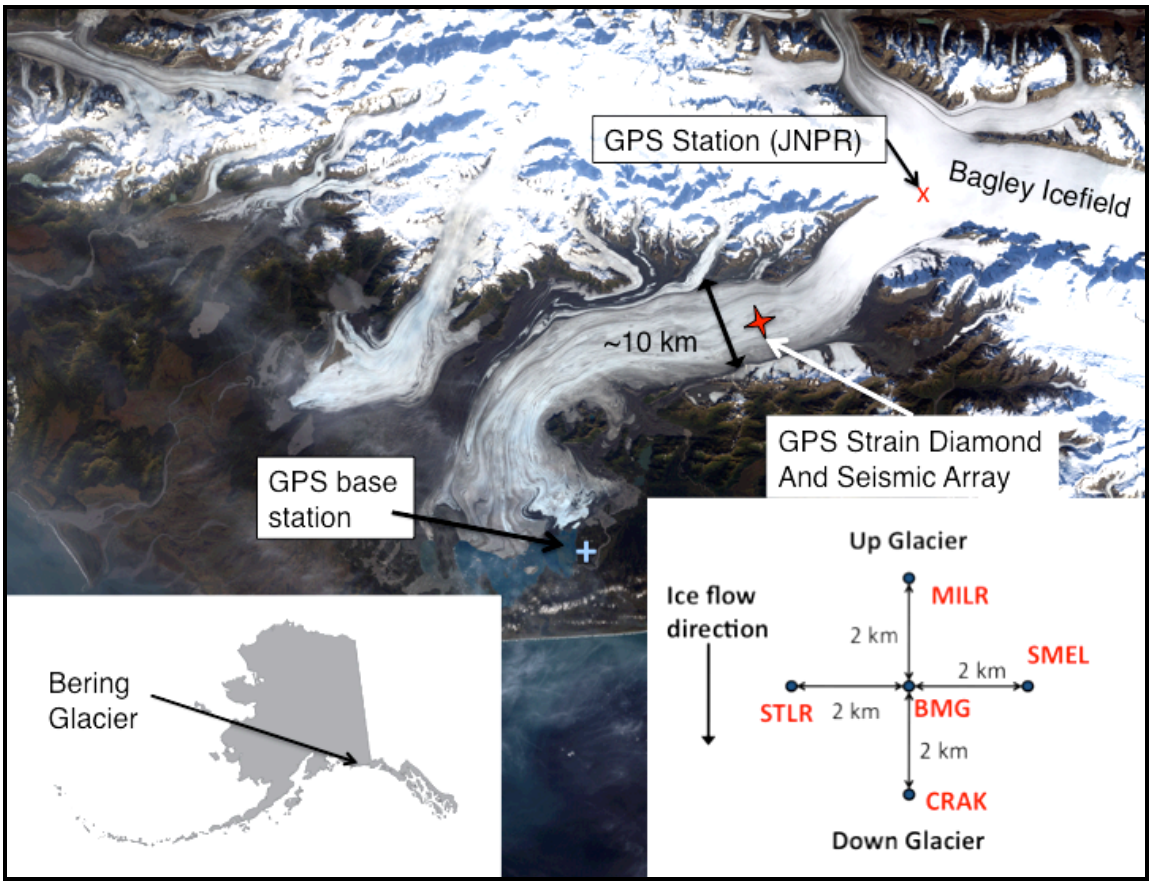

Figure 1. Bering Glacier Location and Site Configuration. The upper GPS station (JNPR) is located near the head of the Bering on the Bagley Icefield. The lower stations (MILR, BMG, CRAK, STLR, and SMEL) are located roughly halfway between the terminus and the equilibrium line, approx. 20 km down glacier from JNPR. Satellite image courtesy of NASA Earth Observatory, September 29, 2002 (http://earthobservatory.nasa.gov/Newsroom/NewImages/Images/bering_etm_2002272_lrg.jpg).

3. METHODS

3.1. GPS

The GPS antennas were fixed relative to the ice, not the free surface, by mounting them on tripods made from 1" diameter plugged steel conduit poles that were drilled 6 m into the ice (Anderson et al., 2004). The GPS installations measured the motion of a point near the ice surface (i.e., at the bottom of the poles) and were independent of surface changes. The motion record results from continuous GPS data recorded at 15-sec intervals.

The dual-frequency GPS data were initially analyzed with Track, a kinematic baseline processing tool developed at MIT as part of the GAMIT/GLOBK GPS Processing Suite (http://www-gpsg.mit.edu/~simon/gtgk/) (Chen, 1999; King and Bock, 2006). In June 2007, our base station receiver at the Bering Glacier Camp had a power failure. This necessitated the use of another more distant GPS base station (EYAC (PBO) at Cordova) with a much longer baseline (~150km), which reduced the solution quality. We performed a second analysis using GIPSY software (Webb and Zumberge, 1995) with simultaneous data from global International GPS Service (IGS) stations. The 5-minute free network solutions were transformed into the International Terrestrial Reference Frame, epoch 2000 (ITRF2000) (Altamimi et al., 2002). The GIPSY solutions were of higher quality compared with the Track record during the period when our base station was not recording. Aside from this period, absolute position estimates for both Track and GIPSY for the kinematic stations agreed to within the noise (~10 cm of data scatter).

Although the Track-processed record had better time resolution with a 15-sec position time series, the better quality 5-minute solutions for site positions from GIPSY were used to calculate the station velocities and strains presented here. The position data was rotated horizontally into a flow-parallel reference frame. To calculate the velocity and the longitudinal strain rates, the 5-minute processed position data was smoothed with a low-pass Chebyshev filter with a four-hr cut-off frequency. Using the 4-hr smoothed data from MILR, CRAK, STLR, and SMEL, local strain rates and velocities were calculated at a central point within the strain diamond (Fig. 1) from mid-summer to early winter of 2007 (7/8 – 12/2/2007).

The standard deviation in the GIPSY-processed horizontal and vertical GPS position measurements is ±4 cm, giving an uncertainty of ±0.3 m d^{-1} in the 4-hr calculated velocity. The Track record was examined for any sudden motions (i.e. > 20 cm within a single epoch), of which

none were found. Although the Track-processed position measurements have 4 cm point-to-point accuracy, reversible displacement of less than approximately 20 cm in one epoch (15 sec) would not be clearly visible above the noise (±10-20 cm).

We used Trimble 5700 GPS receivers with a 15-second recording interval. Two solar-charged lead acid batteries (2 x 100 Ahr) and five back-up air-alkaline dry cell batteries (1200 Ahr at 15V) powered the GPS receivers. The GPS antennas and their tripod mounts were the only equipment exposed above the snow surface prior to summer melt. The receiver and batteries were installed in a water-resistant enclosure at the ice-snow interface under 2-3 meters of snow (JNPR's enclosure was installed on the snow surface).

3.2. Seismic

The seismometers were mounted at the ice surface, buried under ~2-3 m of snow. In July 2007, the five seismometers were replaced with borehole seismometers. The borehole seismometers were placed in 5m-deep holes drilled using a steam drill. Fine light-colored sand was placed in the hole around the seismometer to improve coupling to the ice in the water-filled boreholes. On this temperate maritime glacier, the water in the boreholes likely did not freeze until late fall or early winter.

For seismometers, we used short-period L-22s with a corner frequency of 2 Hz. The L-22 seismic data was recorded and stored on Quanterra Q330 digitizers and balers, respectively. The digitizers recorded the data at 200 samples per second from 4/19/07 to 9/1/07 and were switched to 100 samples per second on 9/2/07 for the remainder of the study. The seismic instruments were powered by six non-rechargeable air-alkaline dry cell batteries (1200 Ahr at 18V).

Due to constraints within both our seismic network and the event characteristics, we were unable to produce reliable seismic source locations. Many of the icequakes were only recorded at one or two stations. Locations are not possible with less than four or five stations, and even with five stations, there may be large associated errors. Many of the events also have no distinguishable P- and S-waves and lack distinct first arrivals, which are necessary for performing standard location algorithms. In this analysis, we instead count the seismic events and investigate their temporal distribution in relation to ice motion on various time scales (hourly – seasonal).

The seismic data set was processed using several STA/LTA (short time average over long time average) detection algorithms. The algorithms evaluate the ratio between short- and long-term energy density to find amplitude transients. Two sets of parameters were designed with different filters and other settings to detect two classes of events, distinguished by their frequency content (Table 1, also Appendix B). The parameters were chosen, based on visual inspection of the seismic record, to better identify two broad categories of waveforms: Low-Frequency (LF) and High-Frequency (HF), which could represent two different groups of source mechanisms. The detection algorithms were run on the vertical channels (EHZ) of the seismic stations. The record from STLR is used for figures and analysis due to its longevity and low noise levels. Because most of the seismic events had relatively broad frequency content, some events may have been detected by both of the detectors.

Table 1. Event Detection Parameters

Detector	Bandwidth	Short Term Averaging Window	Long Term Averaging Window
Low-Frequency	0.8-5 Hz	2.0 sec	10.0 sec
High-Frequency	8-50 Hz	0.2 sec	2.0 sec

In an effort to identify source mechanisms among the thousands of events within the large data set, the LF subset was further processed to look for repeating waveforms. The appearance of a waveform at a given station from a particular seismic event is a result of the source mechanism and the travel path. Seismic events with very similar waveforms can be attributed to the same source location and mechanism. The low-frequency detections were chosen for this analysis for two reasons: 1) based on characteristic frequencies (1-5 Hz) and durations (several seconds to minutes), hydraulic source mechanisms are more likely to be found within this collection than in the HF events (St. Lawrence and Qamar, 1979), and 2) the HF set contains far too many events to make this analysis plausible. We chose two time periods (7/12 – 8/16 and 9/5 – 9/20/2007) for the correlation analysis. The first period was selected to be representative of typical mid-summer dynamics. The second period was selected to provide better insight to dynamics associated with a motion event in mid-September.

We used cross-correlation techniques to measure the similarity of waveforms in the LF dataset. Beginning at each detected arrival time, a 4-second window was extracted from the vertical component (EHZ) of the STLR data. Each waveform was correlated against all other detected waveforms within the given time period using a newly developed algorithm that was designed for working with large datasets and which is part of the Waveform-Correlation toolbox (www.giseis.alaska.edu/Seis/EQ/tools/GISMO/). The waveforms were then grouped into clusters based on a minimum correlation coefficient value.

3.3. Completeness of Record

Routine site inspections and maintenance were conducted in June, July, and September of 2007. In July, it was discovered that several of the enclosures had been flooded during spring melt in mid-June and that some of the GPS and seismic instruments had lost power (SMEL, BMG, JNPR). Local glacier-pilot observations suggest that there was an unusual amount of surface water and snow swamps during spring 2007 (Paul Claus, personal communication, 6/07). Some of the surface-mounted seismometers, due to the lack of overlying snow for support and melting of the underlying ice, had become un-level (MILR: 6/20 and STLR: 7/3). The damaged stations were repaired during the July transition to borehole seismometers. Data gaps in the seismic and motion records from mid-June to early July are due to the power failures and un-level instruments.

With the exception of the period from mid-June to early July 2007, the instruments ran successfully for eight to sixteen months with minimal maintenance. All five GPS receivers were operational from July to November of 2007. By December 2007, some of the receivers had depleted their battery reserves and began to power down (JNPR and CRAK) and by March 2008 all GPS receivers, except STLR, had shut off. The seismic instruments, due to their somewhat lower power requirements, were able to run into late winter of 2008. For both GPS and seismic, station Steller (STLR) produced the longest record. The GPS receiver ran until April of 2008 and the seismometer operated into late July 2008.

4. OBSERVATIONS

4.1. GPS Records of Ice Motion

4.1.1. Horizontal motion

The yearlong GPS horizontal motion record shows spring speed up, diurnal variations in summer, and low velocities in winter. The mean annual velocity of the glacier at the lower stations was 1.2 m d^{-1}. Motion of STLR, which has the longest continuous record and is representative of horizontal motion at the other lower stations, is used in the following discussion and is plotted in Figure 2a.

There was a slow and steady increase in horizontal velocity starting in early May 2007 that was followed in mid-June by the onset of diurnal velocity fluctuations (Fig. 2a). The glacier exhibited diurnal velocity variations until September 9, 2007, when there was a transient increase in horizontal velocity from 1.0 m d^{-1} to 7.9 m d^{-1} within 36 hours (Fig. 2a). This coincided with a large rainstorm recorded at several nearby meteorological stations (Fig. 2d) and was the most substantial velocity increase in the entire data set. The onset of increased horizontal motion at JNPR occurred within several hours of the onset at STLR. The velocity decreased at a rate similar to the speed up, and by September 16 the velocity had dropped to nearly the previous late springtime (4/07 - 5/07) level. After September 9th, there was no diurnal signal in the velocity. With the exception of a few small increases in motion in October and November, the winter velocity was relatively constant at 0.7 m d^{-1} (11/1/07 - 2/15/08), comparable to the spring 2007 rates. From December 2007 to March 2008, there was a monthly fluctuation in the velocity that appears to roughly coincide with the lunar cycle, with several small (+0.2 m d^{-1}) peaks in velocity occurring within 3-6 days after the full moon. The velocity in the late winter of 2008 began a slow increase from 0.8 m d^{-1} in mid-February to 1.2 m d^{-1} in mid-April.

The 2007 onset of diurnal velocity variations roughly coincided with the glacier surface becoming snow-free. A temperature sensor within the Q330 digitizer indicates that the surface was snow free by June 5, 2007 (recognized by the onset of diurnal temperature fluctuations after the insulative snow layer was removed (Kanamori et al., 2008)). Diurnal variations began to be detected in the GPS motion record on June 10th and increased in strength through early July. From July – September 2007, the maximum daily velocity occurred between 5pm and 7pm local

time. The mean summertime velocity was 1.8 m d^{-1}, with maximum values of over 4 m d^{-1} (7/1 - 8/31). The diurnal velocities varied by 50-150% from minimum to maximum. These fluctuations are comparable to the 100% daily variation that was observed on the Kennecott glacier (Bartholomaus et al., 2008). From mid-June to mid-August, there were several three- to five-day periods of increased velocity interspersed with periods of lower velocity.

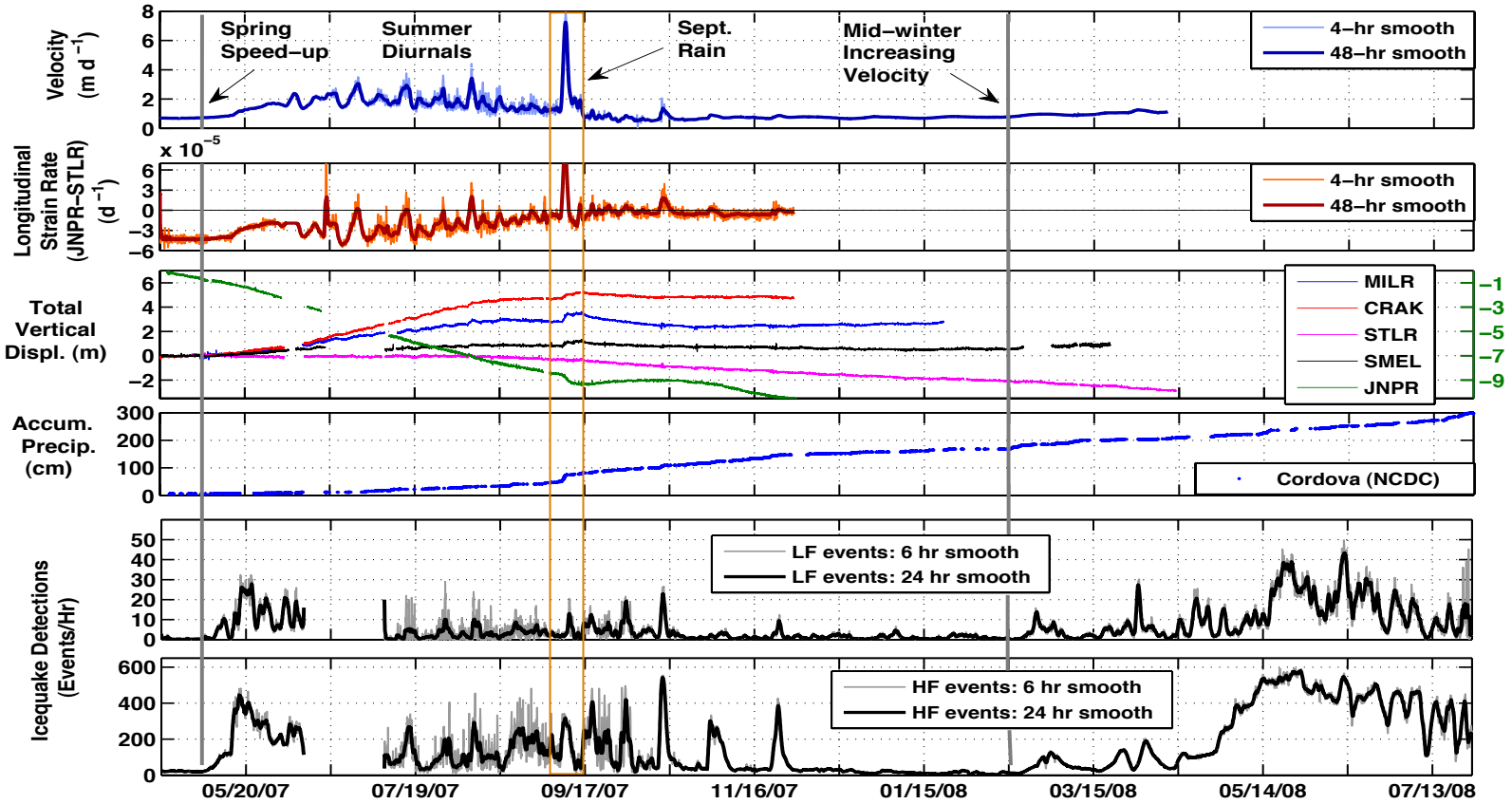

Figure 2. Comparison of ice motion, icequakes, and precipitation showing flow-parallel horizontal velocity from STLR (a), strain rate calculated between JNPR and STLR (b), total vertical displacement (green scale for JNPR) (c), accumulated precipitation (d), and hourly icequake event counts (from STLR) for LF events (e) and HF events (f). Velocity data was calculated from raw positions that were smoothed with a Chebyshev low pass filter (4-hr cut off frequency). All other data was smoothed with a 4-, 6-, 24-, or 48-hour sliding window average. Precipitation data comes from the National Climatic Data Center (lwf.ncdc.noaa.gov/oa/ncdc.html).

4.1.3. Strain Rates

The longitudinal strain rate between JNPR and STLR (located ~20 km apart) ranges from $-4 \cdot 10^{-5}$ d^{-1} to $8 \cdot 10^{-5}$ d^{-1} and shows that the ice flow was predominantly compressional between the Bagley Icefield and the mid-section of the Bering Glacier (Fig. 2b). The flow remained mostly compressional from late April (mean of $-4.2 \cdot 10^{-5}$ d^{-1}) until early September (mean of $-0.2 \cdot 10^{-5}$ d^{-1}) of 2007, with several periods of extension (6/16 –17, 6/27 – 28, 7/13 – 16, 7/27 – 28, 8/6 – 7, 9/8 – 10, 10/11 – 15). The greatest extension ($8 \cdot 10^{-5}$ d^{-1}) was observed following the rainstorm in September. After September 18th, the flow was slightly compressional with strain rates near zero. The early winter average longitudinal strain rate was $-0.2 \cdot 10^{-5}$ d^{-1}. At Taku Glacier, Truffer et al (in press) also found a seasonal reduction in compressional strain rates that was reproduced in a flow model by reducing the strength of the glacier bed.

Local strain rates within the strain diamond (Fig. 1) from mid-summer to early winter of 2007 are shown in Figure 3b & 4b. The ice flow within the strain diamond was largely extensional (extensional 80% of the time with a mean of $1.9 \cdot 10^{-5}$ d^{-1} prior to September and extensional 86% of the time with a mean of $1.8 \cdot 10^{-5}$ d^{-1} after 9/16). An extensional regime is supported by the increase in width of existing crevasses and opening of new crevasses observed near the stations over the duration of the study. The ice flow was also predominantly laterally extensional (extensional 91% of the time with a mean of $1.8 \cdot 10^{-5}$ d^{-1} in mid-summer), although flow became notably less extensional after September 16th (extensional 75% of the time with a mean of $0.6 \cdot 10^{-5}$ d^{-1}). The longitudinal local strain rate (ε_{xx}) ranges from $-15 \cdot 10^{-5}$ d^{-1} to $15 \cdot 10^{-5}$ d^{-1} and the transverse local strain rate (ε_{yy}) ranges from $-5 \cdot 10^{-5}$ d^{-1} to $10 \cdot 10^{-5}$ d^{-1}. The local shear strain rate (ε_{xy}) ranges from $-15 \cdot 10^{-5}$ d^{-1} to $-0.5 \cdot 10^{-5}$ d^{-1}. The components ‘x’ and ‘y’ refer to the horizontal flow-parallel and flow-perpendicular axis.

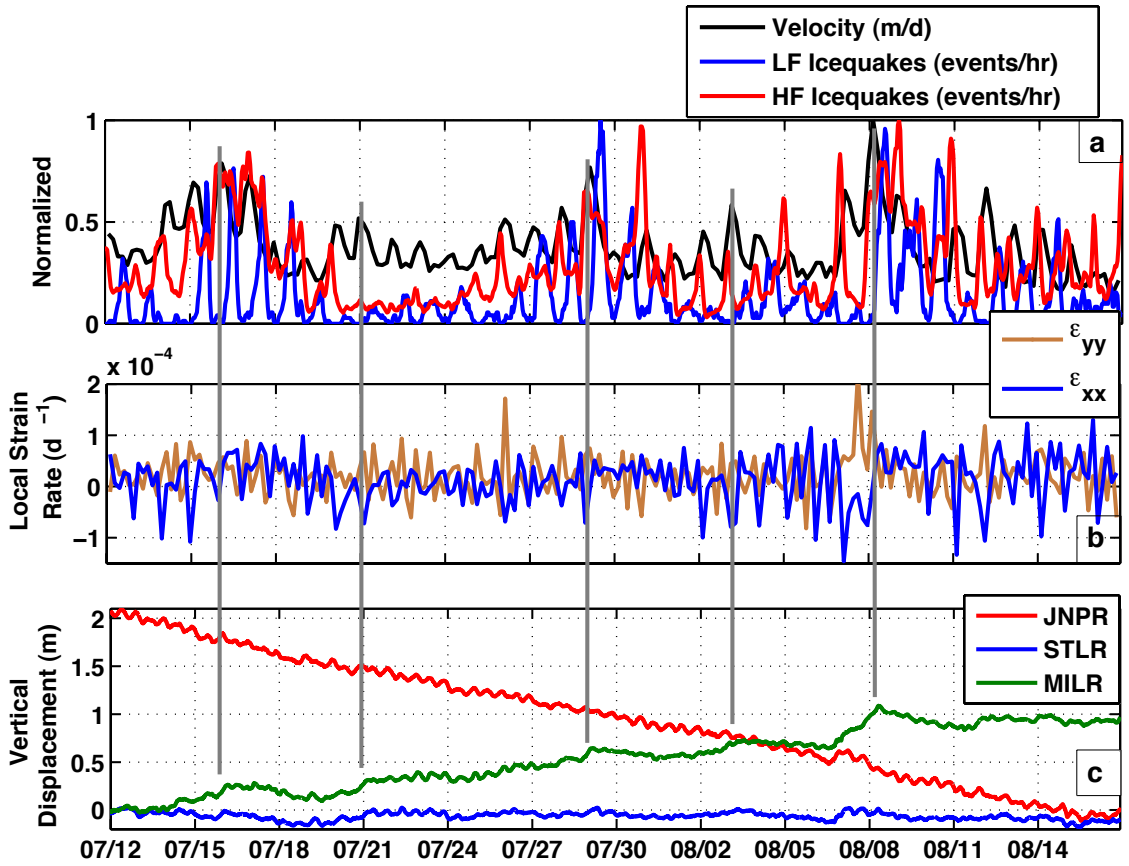

Figure 3. Mid-Summer Comparison of Icequakes and Ice Motion. The horizontal velocity (calculated at a central point in the strain diamond) is plotted with the LF and HF event occurrences (a). Due to several magnitudes of difference in the respective data values (events vs. velocity), the three data sets were normalized to enable plots on the same scale. Local longitudinal (ε_{xx}) and transverse (ε_{yy}) strain rates (also calculated at the strain diamond central point) are plotted in (b). The 'x' and 'y' components have been rotated horizontally and are flow-parallel and flow-perpendicular, respectively. Vertical position data was selected from JNPR, STLR, and MILR to be representative of ice displacements on the upper glacier and on the lower glacier, both near the centerline and closer to the margin (c). The velocity and strain rates were calculated from 4-hr position data. All other data was smoothed with a 4-hr sliding window average. Gray lines mark transient maximums in vertical displacement and are used to compare timing in horizontal velocity, vertical motion, strain rates, and icequake occurrence.

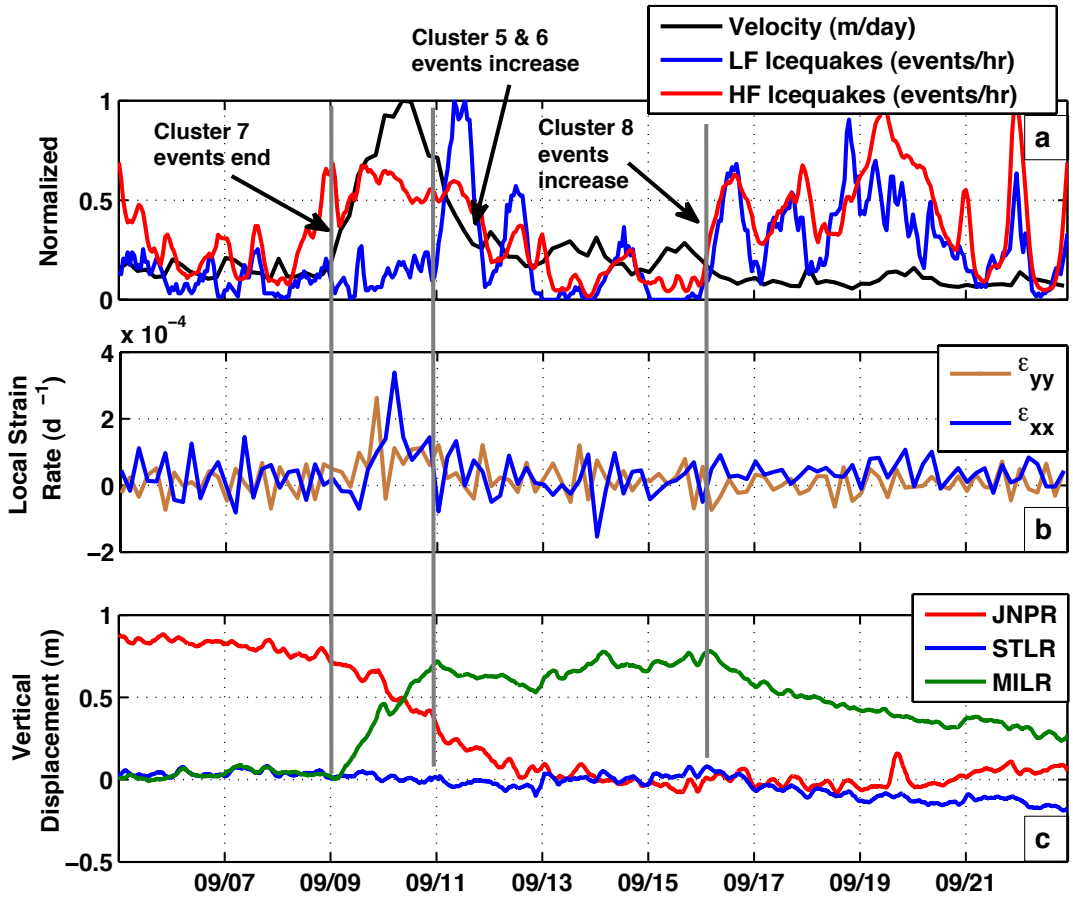

Figure 4. September Comparison of Icequakes and Ice Motion. The horizontal velocity (strain diamond central point) is plotted with the LF and HF event occurrences (a). Local longitudinal (ε_{xx}) and transverse (ε_{yy}) strain rates (strain diamond central point) are plotted in (b). The 'x' and 'y' components have been rotated horizontally and are flow-parallel and flow-perpendicular, respectively. Vertical position data was selected from JNPR, STLR, and MILR to be representative of ice displacements on the upper glacier and on the lower glacier, both near the centerline and closer to the margin (c). The velocity and strain rates were calculated from 4-hr position data. All other data was smoothed with a 4-hr sliding window average. Gray lines mark times of interest and are used to compare timing in horizontal velocity, vertical motion, strain rates, and icequake occurrence.

4.1.2. Vertical Motion

The observed vertical motion in this analysis is a combination of vertical strain, motion parallel to the mean bed slope, dilation of subglacial sediments, and vertical motion of basal ice relative to the bed due to increased basal water (i.e., bed separation). In order to relate ice motion observed at the glacier surface to basal motion, we need to consider the contribution of vertical strain to uplift of ice near the surface (due to ice convergence). Using principles of continuity, the component of vertical motion due to strain at the lower stations was calculated with the longitudinal and transverse horizontal strain rates (ε_{xx} and ε_{yy}) and with an ice thickness of 700 m. Vertical strain within the lower strain diamond can account for approximately -0.15 to +0.10 m d^{-1} of vertical ice motion. Without taking transverse components into account, longitudinal strain rates between the upper (JNPR) and lower stations give approximate strain contributions to vertical displacement of 0.05 m d^{-1} or less.

The most substantial vertical motion within the data set occurred in mid-September 2007, coinciding with the rainstorm (Fig. 2a,d and 4a). Over a two-day period (9/9 - 9/11), there was +45-70 cm of vertical displacement at the center stations on the lower glacier (CRAK and MILR) and it occurred during high rates of extension. The vertical motion following the rainstorm must be due to basal lifting caused by an increase in water storage, presumably at the glacier's base. Downward ice motion began on Sept. 16th and continued into mid-October at MILR, CRAK, and SMEL.

The ice at STLR had begun to move down in mid-August and the steady decline continued into the winter, interrupted only by a transient rise in mid-September (Fig. 2a). The ice at the upper station (JNPR) displayed somewhat different behavior. From April - September 2007, the ice at JNPR showed consistent downward vertical displacement that ended on Sept. 8th. The observed vertical drop of 80 cm during the rainstorm (9/8 - 9/12) was primarily an effect of the large increase in horizontal velocity in an area with a downward surface slope. Extensional strain rates account for no more than 10 cm of the negative vertical displacement at JNPR during this interval. From mid-September to mid-October, there was +40 cm of vertical displacement at JNPR, possibly due to locally increased water storage or a rise in the bed. The ice at JNPR returned to downward motion in mid-October.

In contrast to the vertical motion of the ice at JNPR, the ice moves uphill at the location of the lower stations MILR and CRAK. The uphill slope is likely caused by a large rise in the

glacier bed and is indicative of substantial basal sliding. Compressional strain rates between the upper and lower glacier could also account for ~1 m of vertical displacement throughout the summer (June – September). We recorded total vertical displacements of -8.3 m at JNPR, +4.8 m at CRAK, +3.0 m at MILR, +0.8 m at SMEL, and near zero at STLR (Fig. 2c). There are no apparent diurnal signals in the vertical motion record: short-term (< 1 day) vertical displacements were below the detection limit (± 4 cm).

Several increases in vertical motion at MILR over multi-day periods (e.g. 7/16: 25 cm, 7/21: 25 cm, 7/29: 20 cm, and 8/7: 40 cm) occurred within a few hours of peaks in horizontal velocity (Fig. 3c). The ice at MILR, and then CRAK, shows the greatest vertical fluctuations, compared to fluctuations at STLR and SMEL. There is a suspected depression in the bedrock just up glacier from MILR that is supported by the observation of a surface depression where a large lake forms in the early summer. The middle of the glacier may be more responsive than the sides of the glacier to water input, especially if water is being stored in the underlying depression. Two of the increases (7/16 and 7/29) occurred with extensional flow (Fig. 3b), so are likely caused by increased basal water pressure or storage. The other multi-day increases in positive vertical motion coincided with negative strain rates and are partially due to compressional flow. However, by our calculations, vertical strain could have only accounted for a maximum of +5 cm and +10 cm during the increases of 25 cm (7/21) and 40 cm (8/7), respectively. Thus, increases in water storage likely contributed to the observed positive vertical motion.

4.2. Glacier Seismic Events (Icequakes)

4.2.1. General Characteristics

Both impulsive and emergent arrivals are observed within the Bering seismic data. High frequency (>10 Hz), very short duration (<1 sec) events comprise nearly 95% of the detections. The majority of the other detected icequakes have frequencies of 2-80 Hz and are typically of short duration (1-4 sec), although a few have much longer coda (>100 sec). These characteristics are similar to what has been observed in other glacial seismic studies (Neave and Savage, 1970; Sinadinovski et al., 1999; Deichmann et al., 2000; Metaxian et al., 2003; Gorski, 2004).

The two classes of detected events contain a wide diversity of waveforms. Waveform examples from the LF and HF detection sets are shown in Figure 5. The LF detected events

commonly have peak frequencies of 5-20 Hz and a frequency range of 2-50 Hz. The HF events typically have peak frequencies of 10-40 Hz and a frequency range of 2-100 Hz. The HF events are typically smaller (based on surface displacement measured by seismometers) and shorter in duration than the LF events (0.4 -1.5 s vs. 1.0 - 10.0 s).

The majority of the icequakes within the Bering dataset are quite small, creating surface motion of < 1 mm (as measured by the seismometer). Motion resulting from these icequakes is well below the detection limit of our GPS. There are no large (>20 cm) sudden displacements (over the period of seconds or minutes) in the GPS record. We also do not see any large seismic events like those originating from large glaciers in Greenland (e.g. Tsai and Ekstrom, 2007).

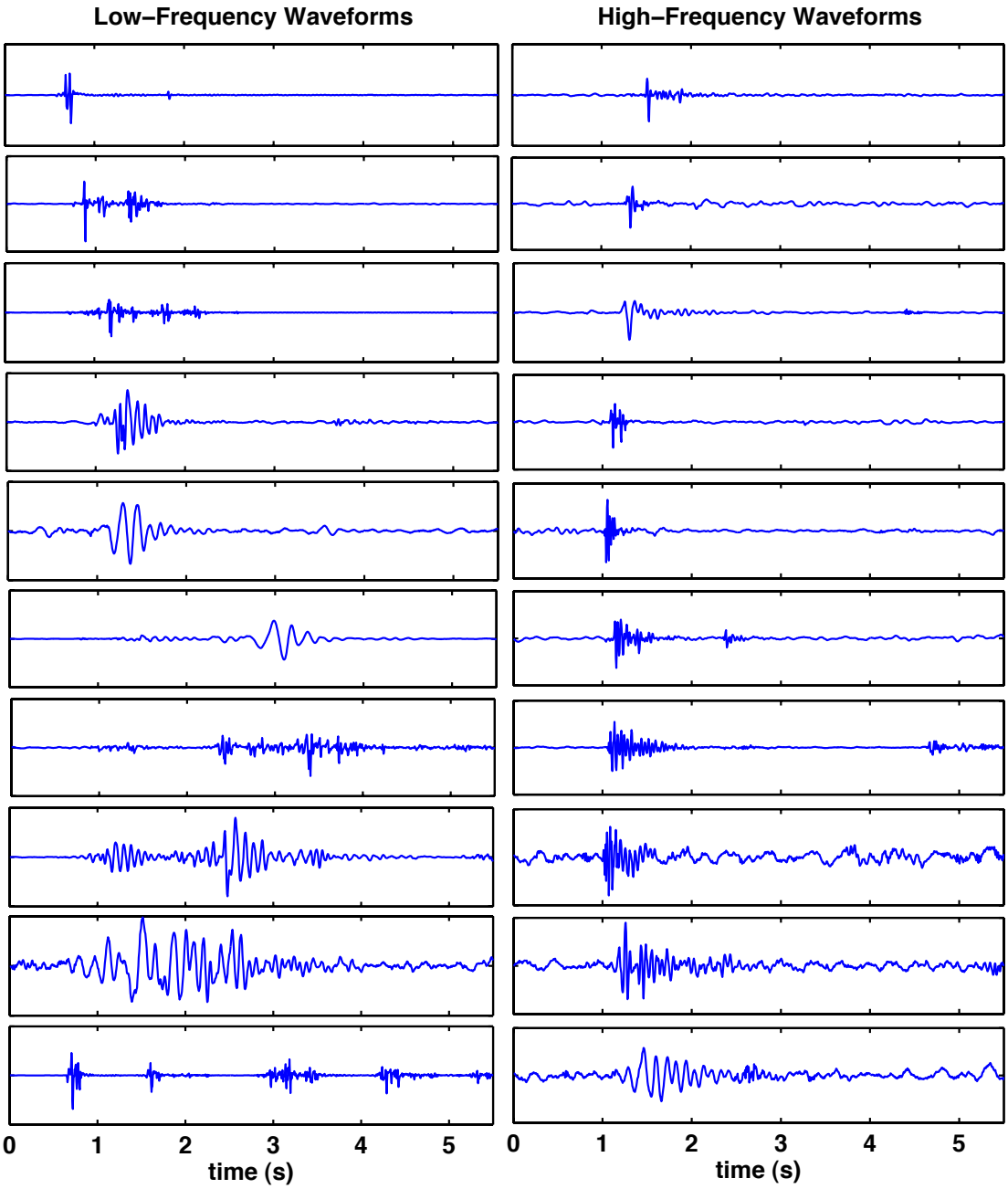

Figure 5. Examples of LF and HF waveforms. These waveforms were randomly selected from the seismic data to be representative of the variety of waveforms present in the LF and HF subsets. Some of these events may be found within both detection sets. The waveforms are unfiltered and plotted on an arbitrary vertical scale. The LF events have typical dominant frequencies of 5-20 Hz and frequency ranges of 2-50 Hz. The HF events have typical dominant frequencies of 10-40 Hz and a frequency range of 2-100 Hz.

4.2.2. Event Detections

We detected over 1.5 million icequake events from April 2007 – July 2008, using STA/LTA detection algorithms (see section 3.2). During periods of high activity, up to 600 HF icequakes per hour were identified (up to 50 LF events/hr). Many of the events are so small (or are attenuated over such short distances) that they were detected on only one or two of the stations. The Bering data was compared with the Alaska Earthquake Information Center (AEIC) regional earthquake catalog to confirm that the majority of these events are relatively small. Such events are not usually detected on the regional network, which consists of bedrock seismic installations in the Bering-Bagley region (Ruppert et al., 2006). However, local and teleseismic earthquakes recorded regionally were also recorded by the glacier stations.

There are three different general behaviors of icequake activity within our data set: high activity in spring, diurnal activity in summer, and low activity in winter (Fig 2e-f). Station STLR (vertical channel EHZ), which ran the longest and with the best quality signal, is used for this analysis. Although there are small variations, the other four seismic stations show similar patterns in event occurrence on daily to seasonal time scales (Appendix A, Fig. 1).

The first onset of icequakes began in early May 2007 with a large increase in seismic activity. The number of detected LF events exceeded 30 per hour (Fig. 2e). The occurrence of HF events show similar temporal behavior, but have much higher hourly detections (up to 450 events/hr) (Fig. 2f). During the spring period, the diurnal signal was weak or non-existent and the peaks in event rates showed no preference to time of day. The heightened level of activity persisted until at least mid-June, after which the seismic data became unusable due to out-of-level seismometers and power failures. By this time, snow melt on the glacier had exposed seismometers on the surface, compromising the instruments and, in some cases, flooding the installations.

The summer record begins on July 9, 2007 (after borehole seismometer installation and site maintenance to restore power). Diurnal event fluctuations and discrete peaks interspersed with periods of low activity characterize this period (Fig. 3a). Summer showed overall lower event counts than during late spring. The difference in behavior between late spring and summer is most apparent during the peak hour of the day, when the maximum number of events occurred (Appendix A, Fig. 2). Although there were some variations during the summer, the peak in occurrence of LF icequakes was detected between 4 am and 10 am local time (App. 1, Fig. 2a).

The HF events show a similar pattern, but occurred several hours later, from 3 – 8 pm local time (App. 1, Fig. 2b).

The diurnal signal disappeared from the seismic record on September 9, 2007, following the rainstorm. A significant increase in seismic events began on September 16th and lasted into early-October. Several peaks in icequake detections occurred during fall and early winter, with the largest peak from Oct. 13th - 17th (LF: 25 events/hr, HF: 550 events/hr). The last two peaks (10/30-11/7 and 11/22-11/26) are much more pronounced in the HF detection record than in the LF record. These peaks were followed by a wintertime quiescence from late November through mid-February. Activity began increasing in late February 2008, with a marked increase in event counts by late April (HF) or late May (LF). Icequake detections were thirty to fifty percent greater in late winter and spring of 2008 compared to the winter and spring of 2007. The strong diurnal signal that was present in summer 2007 is not apparent in the 2008 data. The early summer decrease in events in 2007 is also seen in the 2008 record, although to a lesser degree.

During this study, we essentially had three different seismic installations: ice surface-mounted and buried under snow (4/19/07 – 7/8/07); wet, sand-filled boreholes (7/9/07 - ?); and frozen boreholes (? – 7/27/08). The date of transition from wet to frozen boreholes is unknown, but was most likely sometime in the mid-winter, if not earlier. The environmental differences in these three installations may lead to variances in event detections. A seismometer that is well coupled may be more sensitive to smaller events than a poorly coupled seismometer, and will thus show a higher number of total events. The ratio of the number of large events to total events in the HF counts in Spring 2008 is approximately 50% less than the ratio in Spring 2007. This ratio should remain constant assuming no variance in the network. The change in the ratios in Spring 2007 and 2008 may indicate that the seismic installation in 2007 was not able to measure the smallest events or simply that the two periods produced different seismicity. There may have been more small events in Spring 2008 than in 2007.

4.2.3. Repeating Events

Although the majority of events have unique waveforms, many events with similar waveforms repeat over time. Repeating seismic events with highly similar waveforms indicate repeating source mechanisms (such as a basal sticky-spot or a pinch-point in the hydraulic network). To better recognize these repeating events, cross-correlation techniques were used to

identify similar waveforms within the LF events (see section 3.2). Collections of waveforms with a correlation value of 0.8 or greater were identified as 'Clusters'. Four clusters were selected from each of the two analysis periods (7/12 – 8/16 and 9/5 – 9/20/2007) to be representative of the dominant repeating waveforms (Fig. 6). Specific occurrence dates and hours of daily maximum activity for each of the clusters are displayed in Appendix A, Figures 3 and 4. For a detail of the spectral content of waveforms within each cluster, see Figures 5-12 in Appendix A.

The mid-summer event clusters display much of the same timing, duration, and spectral content as seen in the overall LF events. Clusters 1-3 (Fig. 6a-c) show a strong diurnal occurrence interval, especially pronounced in Cluster 1 (App. A, Fig. 13), and occurred in the morning hours. The events range in duration from 1-3 s (10 s for Cluster 4) and in frequency from 2-40 Hz. The events in Cluster 4 show no significant temporal preference and have very monochromatic waveforms with emergent arrivals (Fig. 6d).

The event clusters in September indicate a possible shift in fall icequake activity and emphasize the increase in LF event occurrence that began on September 16th. The Cluster 7 events (Fig. 6g), which also likely occurred during the summer (similar to Cluster 3), do not occur after September 9th. Clusters 5 and 6 (Fig. 6e-f) increased in occurrence on September 12th and by September 16th, showed a strong increase. The Cluster 8 events (Fig. 6h), which have impulsive arrivals and no daily temporal dependence, occur primarily after September 16th and are not found as repeating waveforms in the mid-summer period. With the exception of Cluster 8, the cluster events of the September period are nearly identical in frequency content, duration, and waveform shape to the cluster events of the mid-summer period. However, the event rate in the clusters of the second period reveals much less preference to the hour of the day and shows little-to-no consistent diurnal interval.

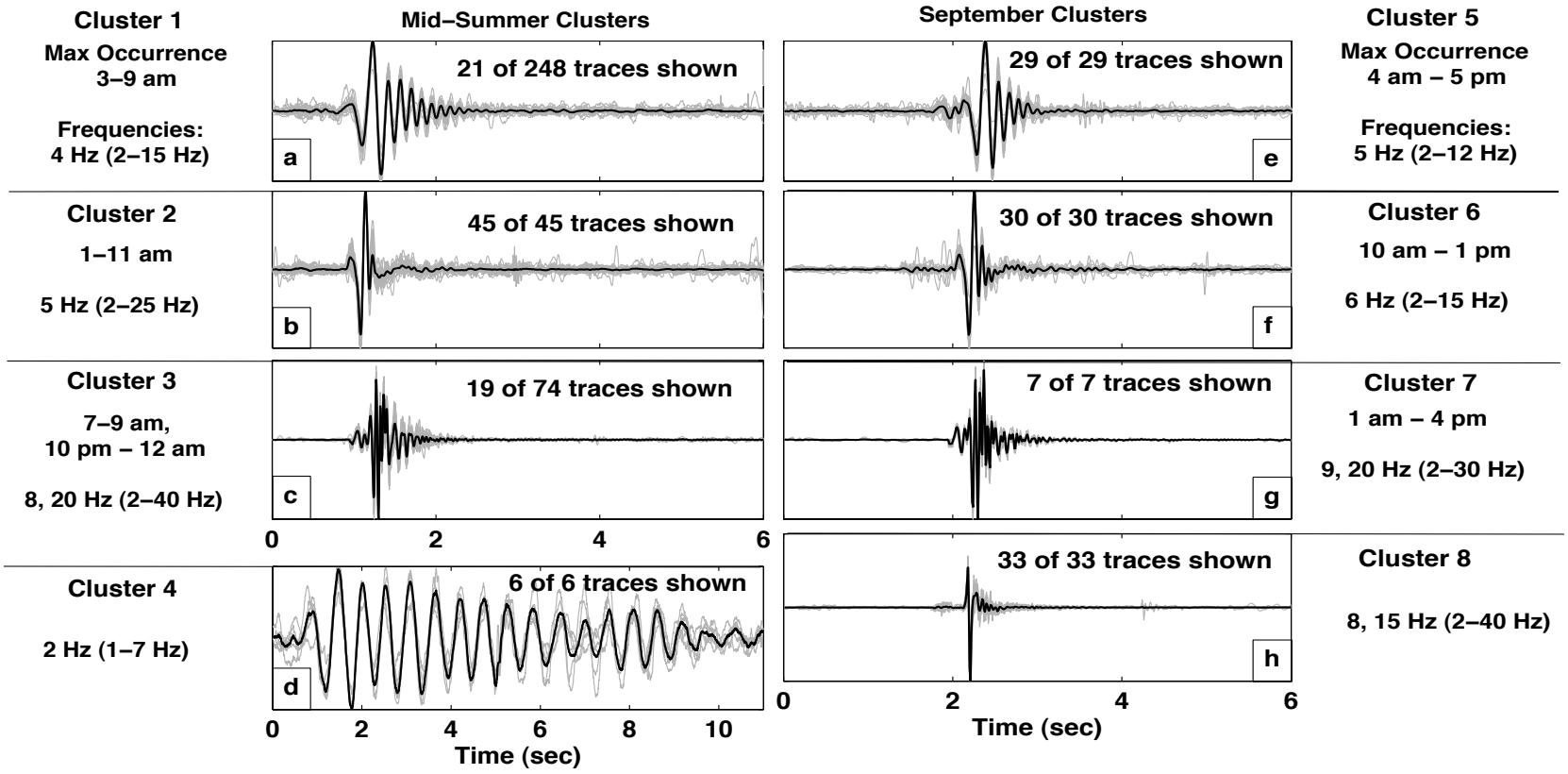

Figure 6. Mid-Summer and September Waveform Clusters. The time of day at which the maximum number of icequakes occur, as well as the peak frequency and frequency range, is listed for each cluster. The light gray lines are the traces of the individual waveforms and the overlying black line is the stack of all waveforms shown. Note that the timescale for Cluster 4 is different than the other plots.

5. DISCUSSION

5.1. Relation of Icequakes, Ice Motion, and Basal Hydrology

We have observed variations in glacier horizontal and vertical motion on diurnal to seasonal timescales. Many studies have made similar observations on other glaciers and have used fluctuations in glacier motion measured on the surface to infer basal motion variations (Willis, 1995). Variations in basal motion can be a result of changes in subglacial water pressure or water storage (Iken et al., 1983; Kamb et al., 1994). Here, we apply what has been learned from such studies on the relationships between velocity variations and the development of the hydraulic network to our own observations of the correlation between ice motion and icequake activity to gain a better understanding of the basal hydraulic system and associated source mechanisms on the Bering Glacier.

5.1.1. Winter Quiescence to Summer Diurnals

The onset of increased velocity and icequake activity during early May indicates probable changes in basal conditions. Spring speed-up has been observed on many glaciers and is thought to reflect an initial disruption of the winter subglacial drainage configuration by the new influx of melt water (Hubbard and Nienow, 1997). At the beginning of the melt season the drainage system, which may consist of a network of poorly connected cavities, has low capacity. As surface-derived meltwater is first supplied to the glacier bed via moulins and crevasses there is an increase in subglacial water storage that results in increased basal motion. This is attributed to increased pressurization of the subglacial drainage system that leads to increased separation from the bed, decreased basal friction, and enhanced basal motion. This increase in water storage causes the winter distributed network to evolve into larger connected channels (Fountain and Walder, 1998). We propose that the large increase in seismicity during spring is most likely related to this reorganization of the glacier's hydraulic system and associated changes in the basal stress regime.

The transition from spring speed up (5/12-6/5/2007) to strong diurnal fluctuations by early July likely reflects the development of a well-connected and distributed drainage system. Our evidence is the strong correlation between the "snow-free" date (June 5) and the onset of

diurnal variations in the motion record. This correlation indicates a connected system in which most of the surface water input is routed directly to subglacial channels. Once the snow has melted, the water flux into the glacier should have large diurnal variations caused by diurnal fluctuations in melt rates (Nienow, 1994) and conduits may only be pressurized for a short time each day. The added basal water pressure would cause the diurnal increase in velocity.

The springtime distribution of event detections in 2008 appears to continue later into the summer than in 2007, which may be associated with different conditions between the two years. In 2007, the glacier surface in the vicinity of our lower stations was snow-free by late June. It was a colder, snowier spring and summer in 2008 and the glacier surface was not snow-free that year until mid-August. Typical springtime glacial dynamics may have extended much later into the summer of 2008. The contrast in behavior of the seismicity in the early summer of 2007 and 2008 suggests that surface melt and a developed network of moulins are needed to produce the transition to diurnal event occurrence and related motion. A multi-year record is needed to test this hypothesis.

5.1.2. Summer Dynamics

Surface melt rates are primarily controlled by solar radiation and, therefore, the greatest amount of melt water production likely occurs during the daily maximum in solar radiation (Röthlisberger and Lang, 1987). In the summer months near the Bering Glacier, this maximum occurs between 11 am and 2 pm local time (WRCC-RAWS data, www.raws.dri.edu). In contrast, the velocity peaks are on average between 5pm and 7pm. If this velocity variation is caused by meltwater input, then the transit time for meltwater to the bed must be on the order of a few hours. Such short transit times from surface to bed were found in moderate-sized temperate glaciers by Fountain and Walder (1998). In studies on the Kennecott Glacier, Bartholomaus et al. (2008) estimated two hours to be a reasonable time for supraglacial melt to reach the subglacial system, assuming a 2.5 km mean travel length to nearest moulin and 0.5 ms^{-1} supraglacial channel flow speed. Although Kennecott is also a temperate Alaskan glacier, at approximately 40 km long and several kilometers wide, it is considerably smaller than the Bering. The Kennecott is also subject to an interior climate in contrast to the maritime climate of the Bering. With a depth of ~700-1000 meters on the Bering Glacier, it is reasonable to expect longer travel times for

water moving from surface to bed, provided that the water is travelling along a gradually descending path and not in direct vertical channels.

A strong diurnal signal is present in both the velocity record and the icequake detections from mid-June to late August 2007 (Fig. 3a). LF events occurred during decreasing or minimum velocities and HF events occurred during increasing or maximum velocities. For the discussion within this section, we refer to the 4-hr velocity calculated at a point central to the lower stations (roughly at BMG). The HF counts are roughly in phase with the velocity peaks in July (range of ± 2 hrs) and precede the velocity peaks by 2-3 hours (± 2 hrs) in August (Appendix A, Fig. 14b). The daily peaks in LF counts are roughly out of phase, corresponding with decreasing or minimum daily velocities. The maximum LF event counts occurred 10 hours (± 5 hrs) after the velocity peaks (Appendix A, Fig. 14a). The event timing in the repeating waveforms of Clusters 1-4 echoed what was observed in the total LF event counts and typically occurred at decreasing or minimum daily velocities (Fig. 7a). Cluster 3 of this class occurred primarily during large (15 – 25 cm) negative vertical displacements (Fig. 7b). The difference in relation to velocity between the LF and HF events supports the argument for two distinctly different groups of source mechanisms that produced the events. As examples, the HF events could be attributed to mechanisms associated with increasing ice motion (i.e. crevassing), whereas the LF events may be produced by mechanisms related to decreasing motion (i.e. changes in the basal hydraulics or till failure due to basal recoupling).

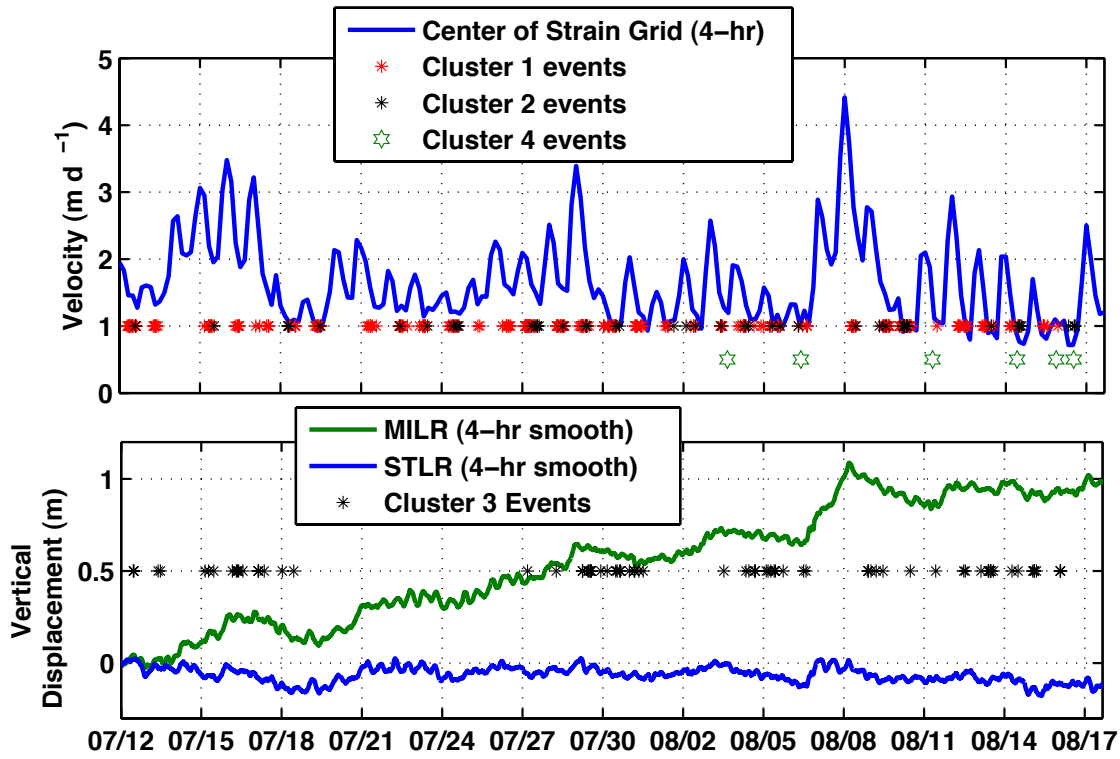

Figure 7. Comparison of repeating events and ice motion. Horizontal ice velocity (calculated from 4-hr positions at a point central to the strain diamond) is compared with detection times of repeating waveforms from Clusters 1, 2, and 4 (a). The detection times of Cluster 3 are compared with the vertical displacement (4-hr sliding window average) at two stations on the lower glacier (MILR and STLR) (b). Clusters 1,2, and 4 typically occurred during decreasing or minimum velocities and Cluster 3 occurred primarily during negative vertical motion.

5.1.3. Rainstorm and Reorganization

On September 8, 2007 there was a major rainstorm in which the weather station at Bering Glacier Camp measured accumulation of nearly 30 cm in a 24-hour period (Fig. 2d). This rainstorm coincided with the largest velocity peak (up to 8 m d^{-1}) at all stations and the largest vertical displacement at the centerline lower stations (MILR: +70 cm and CRAK: +45 cm) (Fig. 2a and c). The increase in the rate of vertical displacement (-80 cm over a 4-day period) of the ice at JNPR was mostly attributable to the velocity increase. There was a major increase in longitudinal (JNPR-STLR) and local strain rates ($1.2 \cdot 10^{-4}$ d^{-1} and $3.4 \cdot 10^{-4}$ d^{-1}) that peaked several

hours prior to the September 10th velocity maximum (Fig. 2b and 4b). Extension during the uplift event at the lower stations indicates that the vertical displacement was most likely caused by an increase in basal water pressure and storage during the rainstorm. The much greater vertical displacement observed at the centerline stations (MILR and CRAK) may be explained by larger water storage in this area, due to the reverse slope of the glacier and possible local over-deepening of the bed.

The effect of the September rainstorm on the ice velocity was possibly due to both the intensity and total amount of precipitation, as well as the timing relative to the state of the hydraulic network. It is possible that prior to the rainstorm the basal drainage system was evolving back to a lower capacity configuration. A reduction in meltwater input with cooler weather in late August or early September would have promoted the collapse of the larger basal conduits and cavities. A reduction in volume at the base due to conduit collapse would transfer to negative ice displacement near the surface. This is supported by the shift observed in the vertical displacement of the lower stations in mid-August when positive vertical displacement reached a plateau at MILR, CRAK, and SMEL. At this time, there was also an onset of negative vertical displacement at STLR. Following this period of conduit collapse, a large influx of rainwater flooded the relatively low capacity system, causing greater ice-bed separation, a reduction in effective basal roughness, and a resultant large increase in basal motion.

There is a significant shift in dynamics following the rainstorm as evidenced by the much lower velocities, negative vertical motion, higher seismic event counts (possibly due to bed recoupling), and absence of a diurnal signal in both the motion and the seismic records. A trigger for drainage system reorganization may be provided by a heavy summer rainstorm or ice-marginal lake drainage (Hubbard and Nienow, 1997; Bartholomaus et al., 2008). The large influx of water may have caused an increase in size of channels and cavities (Fountain and Walder, 1998). In the absence of high water input, these enlarged channels and cavities would have collapsed. The downward vertical motion of the lower stations, which began on Sept. 16th, could have been caused by a decrease of volume in the basal drainage system (Fig. 2c and 4c).

The timing and level of event detections, as well as the relation between seismicity and ice motion, also suggest a shift in dynamics following the rainstorm. A noticeable increase in events began on September 16th, at approximately the same time that the velocity decreased to near wintertime levels (< 1 m d^{-1}) and the vertical displacement became negative at the lower stations (Fig. 4). The appearance of some clusters of repeating events and the disappearance of

others also occurred at this time (Fig. 4, also Appendix A, Fig. 11). Cluster 8 is not found as a predominant repeating waveform in the summertime and may be indicative of a mechanism that occurred more frequently in the fall. This shift in dynamics is further supported by occurrence of the Cluster 7 waveforms, which were likely present in the summer events (Cluster 3) and which disappeared after the rainstorm.

There was a greater lag time between event detections and velocity maximums during the rainstorm than in the summer months. The peak in HF icequakes that is associated with the 8 m d^{-1} peak in velocity occurred about six hours prior to the initial increase in velocity, which is nearly a day and a half before the peak in velocity. As during the summer months, the peak in LF events followed the maximum velocity, but by a longer lag of a little over a day. After September 16th, there was much lower correlation between ice motion and icequakes.

The largest increase in velocity of the entire data set coincided with a comparatively small peak in seismic activity. During the summer months, the sizes of the peaks in icequake detections are typically proportional to the sizes of the associated peaks in velocity. This is not the case during the rainstorm when the peak in icequake activity was equal to or less than during the much smaller mid-summer peaks in velocity.

Up until the September rainstorm, we had found no significant correlation of ice motion or icequake occurrence with precipitation or temperature (except on diurnal timescales). This could imply that the percentage of influx due to summertime diurnal melt is far greater than that due to precipitation. From June – August 2007, no rainfall produced more than 5 cm w.e. in a 24-hr period (Fig. 2d). In contrast, the average amount of ablation near our stations is ~4 m w.e. (personal communication, Edward Josberger, USGS, 8/08). Given an ablation season of approximately 90 days (6/10 – 9/ 10), average daily melt input would be ~5 cm w.e. However, the daily amount greatly fluctuates with varying weather conditions (e.g. solar radiation, wind, and temperature).

There was no apparent diurnal signal in either the velocity or the seismic detections after the rainstorm. The lack of diurnal signal in the motion and seismic records may have been due to the destruction of summer networks by the massive influx of water, leaving a new configuration that did not produce variations in basal motion from diurnal water inputs. The diurnal influx of surface meltwater would have also ceased by about this same time. The temperature record at the seismic stations loses a diurnal signal by October 20, signifying the beginning of the winter's snow accumulation.

5.1.4. Winter Dynamics

The relationship between icequakes and ice motion in the late fall and early winter is notable in that there are large peaks in event detections that correspond with comparatively very small increases in velocity. This new relation between seismicity and motion began after the September rainstorm. Some of the highest seismic event rates of 2007 occurred in mid-October (10/13 – 17) in conjunction with a small increase in velocity (Fig. 2). This period also coincided with increased extensional strain rates ($4 \cdot 10^{-5}$ d^{-1} longitudinal, $15 \cdot 10^{-5}$ d^{-1} local). There are several other small increases in velocity that correlate with very high event counts, and which also correspond to small increases in longitudinal and local extension.

The reasons for the seasonally high seismic event detections in relation to small velocity increases in October and November are not well understood. The decrease in the volume of the basal hydraulic network, as suggested by the downward vertical ice motion of the lower stations, may create more contact surface area or better coupling between the ice and the bed (either till or bedrock). Truffer and Harrison (2006) found that ice motion during periods of low water pressure might indicate shearing of basal sediments rather than glacier sliding.

The marked increase in icequake activity that began in mid-February 2008 signifies another possible shift in dynamics. The onset of the increase coincided with a slow and steady increase in horizontal velocity (Fig. 2). Similar to the events in October and November 2007, reasons for the high event rates and the associated mechanisms for the mid-winter seismicity are not well understood. The seismic events may reflect changes in the hydraulic network and basal stress regime that would cause the increase in velocity. As the basal network collapses through the fall and early winter in response to decreasing water input, the storage capacity is reduced. As water slowly accumulates in the basal network through the winter, the pressure in the cavities may increase, leading to increased basal motion.

5.2. Proposed Icequake Source Mechanisms

Possible source mechanisms for icequakes are calving (Qamar, 1988; O'Neel and Pfeffer, 2007), crevassing (Neave and Savage, 1970; Deichmann et al., 2000), basal slip (Weaver and Malone, 1979; Anandakrishnan and Bentley, 1993), basal fracture (Walter et al., 2008), fluid-

induced crack propagation (Metaxian et al., 2003), and hydraulic transients (water hammer) (St. Lawrence and Qamar, 1979; Metaxian et al., 2003). The relationships between ice motion, basal hydrology, and the timing of icequake events, as well as individual clusters of repeating icequakes, can provide evidence for possible mechanisms within the Bering data set. In this section, we explore several viable mechanisms that may be attributable to the HF events and to specific waveform clusters representative of the LF events.

5.2.1. Calving

Bering Glacier terminates in Vitus Lake, where icebergs frequently calve. However, in comparison to tidewater glaciers (O'Neel and Pfeffer, 2007), calving is not seen as a dominant source of seismic events within our record. There are very few events within the Bering record that resemble calving events similar to those originating from Columbia Glacier or glaciers within Icy Bay recorded by the AEIC seismic network (Shad O'Neel, personal communication, 10/09).

5.2.2. Crevassing

Crevassing is a consequence of glacier dynamics and has a relatively high rate of occurrence. In a number of seismic studies, many of the near-surface sources were attributed to crevassing (Neave and Savage, 1970; Anandakrishnan and Bentley, 1993; Deichmann et al., 2000; Metaxian et al., 2003). These events tend to be of comparatively high frequency (>10Hz), very short duration (<1s), and have impulsive onsets. Many hundreds of such events are observed every hour in the Bering data, especially within the HF detection class. The events are often recorded by only one seismic station, implying that they are not highly energetic. For events that appear at only one station and given our station spacing of 2 km and a local ice thickness of ~700 m, the source to receiver travel distance should be less than 2 km. The events occurred primarily during increasing or maximum velocity, when crevassing rates are expected to be high.

5.3.2. Hydraulic Transients

The velocity and seismic records indicate that the englacial and basal drainage systems are continuously changing (Fountain and Walder, 1998; Bartholomaus et al., 2008). Any change in a steady-flow condition will generate a transient response. Röthlisberger (1972) suggested that connections between intraglacial and subglacial conduits might act to valve fluid flow. Transient disturbances of water flow within the glacier may cause fluctuations in the fluid pressure, which result in displacement of the conduit walls (St. Lawrence and Qamar, 1979). Oscillatory pressure, similar to that which generates the 'water hammer' effect in plumbing systems, displaces the conduit wall, providing impulse for the observed harmonic signal (Wolf and Davies, 1986; Kavanaugh and Clarke, 2001). The length of the conduit through which the pressure wave travels will determine the frequency of the resultant waveform (St. Lawrence and Qamar, 1979; Metaxian et al., 2003). Hydraulic transients have been ascribed to waveforms with emergent onsets, weakly developed or no seismic phases (P- and S-waves), and monochromatic frequency spectrums (St. Lawrence and Qamar, 1979).

This mechanism is consistent with the emergent onset and relatively narrow frequency range characteristic of the repeating waveforms in Clusters 1, 4, and 5. Due to the high correlation value (>0.8) of all the waveforms within each cluster, we can assume that all of the events from within each cluster originate from the same location (Buurman and West, in press). Crevassing and fluid-induced ice fracture can both be discounted as possible mechanisms. The majority of the events occur in the early morning hours during local extensional flow, although some occur under compression. Crevassing events typically occur during periods of extension or high shear strain. However, due to the non-impulsive, LF (3-7 Hz dominant) characteristics of Clusters 1, 4, and 5, it is unlikely that crevassing is the source of these events. The morning velocity minimum suggests that there is a daily minimum in the subglacial water pressure. The time of day that the maximum number of the Cluster 1 events occur (3-9 am) suggests that we can therefore discount hydrofracturing as a mechanism as it would be most likely to occur when basal water pressure is high (Walter et al., 2008).

Clusters 1, 4, and 5 have diurnal occurrence (primarily Cluster 1), show a direct relation to periods of decreasing velocity, and little preference to the magnitude of the velocity (Fig. 7 and App. A, Fig. 15). On a glacier as thick as Bering (~700 m), subglacial channels will begin to close on the order of several hours after a decrease in water flux (Nienow et al., 1998; Bartholomaus et al., 2008). Changes in the configuration of the basal network (e.g. collapsing

conduits or shifting drainage pathways) may create disruptions in water flow that would cause pressure waves, or hydraulic transients.

5.3.3. Basal Failure

Like Cluster 1, the repeating waveforms in Clusters 3 and 7 also occur in the early morning, typically at or near velocity minimums (Fig. 7 and App. A, Fig. 11). However, they have more impulsive arrivals, higher spectral content (10-19Hz peak, 2-35Hz range), and less harmonic waveforms. As the glacier slows, it may recouple to the bed, causing tensile fracturing in the ice or substrate (Walter et al., 2008). Sliding would then drive fracture of the newly coupled ice and till, possibly resulting in stick-slip motion. This mechanism has been ascribed to small seismic events like those in Clusters 3 and 7 (Walter et al., 2008). The waveforms of Clusters 3 and 7 are also similar to events observed at Mawson Station, which were attributed to ice fracture (Sinadinovski et al., 1999).

Cluster 8 shows a notable increase in event rates after September 16. The onset of increased seismicity of this group coincided with the start of negative vertical ice motion that began after the large vertical maximum (Fig. 4 and App. A, Fig. 15). These waveforms are unlike any other clusters, exhibit P- and S-wave phases, and may represent a mechanism that is not common during the summer. Based on their timing, impulsive arrival, and somewhat higher frequency content, they could be ascribed to mechanisms associated with till failure or recoupling to the bed.

6. CONCLUSIONS

Results from a year and half long deployment of seismometers and GPS receivers on the Bering Glacier, Alaska, have provided us with the clues to better understand the evolving daily and seasonal dynamics of a temperate glacier. The Bering produces many icequakes (up to 600 events/hr) and exhibits diverse waveforms associated with a dynamic system. The majority of the icequakes are quite small with very short durations (0.5 – 3 s) and frequency contents of 2-90 Hz (the L-22 seismometers have a corner frequency of 2 Hz). The GPS motion record gives a mean annual horizontal velocity of 1.2 m d^{-1} and shows evidence of a spring speed-up, diurnal velocity fluctuations in summertime with peaks of up to 4 m d^{-1}, and winter quiescence. A major fall rainstorm is associated with the most substantial transient increase in horizontal velocity (8 m d^{-1}) and vertical ice motion (+70 cm). During the summer months, positive vertical displacements of 20-40 cm over the period of a few days occur during periods of increased horizontal velocity. These vertical displacements cannot be fully explained by compressional strain rates and are likely associated with increased water pressure in the basal hydraulic system. A strong relationship between ice motion and icequake occurrence exists during spring speed-up, summer diurnal motion, and winter quiescence on the Bering Glacier.

The variations in event counts and ice velocity through the data set are likely a direct effect of seasonal changes in water input. Several distinct shifts in horizontal velocity, vertical ice motion, and icequake occurrence indicate that the glacial hydraulic network is a continuously changing system. We have observed a spring speed-up and an onset of diurnal motion echoed in the icequake event counts. The correlation between the melt of the winter snowpack and the onset of diurnal velocity variations at our stations suggests the development of a connected system, in which most of the surface water input is routed directly and efficiently to subglacial channels. This is further supported by the close timing of daily maximum surface melt water production and maximum daily velocity during the summer months. Based on the strong diurnal signal present in both the icequake and motion records, it appears that melt water input dominated the 2007 summer dynamics on the Bering Glacier. Given the right timing during the development of the hydraulic network, large influxes (from rainstorms or other sources) can also have a dramatic effect on the subglacial hydrology and the surface velocity. The major increase in velocity associated with the September rainstorm was likely a response to a large influx of water in a relatively low-capacity drainage network.

The seismic events have been grouped into two broad categories based on duration and spectral characteristics, which we have distinguished as Low-Frequency (LF) and High-Frequency (HF) events. Hourly event counts were produced for both groups of events. A distinct correlation was found between icequake occurrence and ice motion. The difference in the relation to velocity between the LF and HF events is evidence that the two classes are representative of two different categories of source mechanisms within the data set. The LF events generally occurred in the early morning and coincided with decreasing or minimum velocities. The HF events are shorter in duration and occurred in the late afternoon or early evening. Maximum daily occurrence of the HF events coincided with increasing or maximum velocities.

We attribute crevassing to the source mechanisms that produce a majority of the HF events, due to their short duration, relatively high-frequency signal, and occurrence during heightened velocities. Using cross-correlation techniques to identify similar waveforms, we examined repeating events within the LF detection set to establish predominant possible mechanisms, based on waveform characteristics and timing in relation to ice motion. We find hydraulic transients, till failure, basal fracture, and basal recoupling to be plausible mechanisms within the Bering data set.

There was an apparent shift in the dynamics after the September 8th rainstorm. The decrease in surface velocity, onset of negative vertical motion, and heightened icequake activity, along with the lack of diurnal signal in both velocity and icequake event counts, indicates a transition in the subglacial network and associated basal conditions. This change in dynamics is also signified by the alteration in icequake occurrence shown both by the presence of specific repeating events and by the relation to ice motion. Clusters 3 and 7 disappeared after the rainstorm, while Cluster 8 became much more prevalent. During the summer months, the sizes of the peaks in icequake detections are typically proportional to the sizes of the associated peaks in velocity. This is not the case after the rainstorm. Small increases in fall and winter velocity coincided with proportionally much higher seismic event rates.

A surprising finding from this study is the high level of icequake activity in the late winter of 2008. The increase in event rates coincided with slowly rising velocities. This may indicate that there was some basal reorganization that occurred much earlier than that associated with the expected spring speed-up. The icequakes may also be a sign that there was water flow in

the hydraulic system throughout much of the winter. This development in the glacier dynamics may have gone unnoticed if examining the motion record alone.

REFERENCES

Altamimi, Z., P. Sillard and C. Boucher. 2002. ITRF2000: A new release of the international terrestrial reference frame for earth science applications. *J. Geophys. Res.*, **107**(B10), ETG2.1-ETG2.19. DOI:10.1029/2001JB000561.

Amundson, J.M., M. Truffer, M.P. Luthi, M. Fahnestock, M. West and R.J. Motyka. 2008. Glacier, Fjord and seismic response to recent large calving events, Jakobshavn Isbrae, Greenland. *Geophysical Research Letters*, **35**(L22501), doi:10.1029/2008GL035281.

Anandakrishnan, S. and C.R. Bentley. 1993. Micro-Earthquakes beneath Ice Stream-B and Ice Stream-C, West Antarctica - Observations and Implications. *Journal of Glaciology*, **39**(133), 455-462.

Anderson, R.S., S.P. Anderson, K.R. MacGregor, E.D. Waddington, S. O'Neel, C.A. Riihimaki and M.G. Loso. 2004. Strong feedbacks between hydrology and sliding of a small alpine glacier. *Journal of Geophysical Research-Earth Surface*, **109**(F3), -.

Bartholomaus, T.C., R.S. Anderson and S.P. Anderson. 2008. Response of glacier basal motion to transient water storage. *Nature Geoscience*, **1**(1), 33-37.

Beedle, M.J., M. Dyurgerov, W. Tangborn, S.J.S. Khalsa, C. Helm, B. Raup, R. Armstrong and R.G. Barry. 2008. Improving estimation of glacier volume change: a GLIMS case study of Bering Glacier System, Alaska. *The Cryosphere*, **2**, 33-51.

Buurman, H. and M.E. West. in press. Seismic precursors to volcanic explosions during the 2006 eruption of Augustine Volcano. *The 2006 eruption of Augustine Volcano: U.S. Geological Survey Professional paper*, Ch. XX.

Chen, G. 1999. GPS kinematic positioning for the airborne laser altimetry at Long Valley, California. (PhD Thesis MIT.).

Conway, H., B. Smith, P. Vaswani, K. Matsuoka, E. Rignot and P. Claus. 2009. A low-frequency ice-penetrating radar system adapted for use from an airplane: test results from Bering and Malaspina Glaciers, Alaska. *Annals of Glaciology*, **50**(51), 93-97.

Daly, C., R.P. Neilson and D.L. Phillips. 1994. A statistical- topographic model for mapping climatological precipitation over mountainous terrain. *Journal of Applied Meteorology*, **33**(2), 140-158.

Deichmann, N., J. Ansorge, F. Scherbaum, A. Aschwanden, F. Bernardi and G.H. Gudmundsson. 2000. Evidence for deep icequakes in an Alpine glacier. *Annals of Glaciology*, **31**, 85-90.

Fountain, A.G. and J.S. Walder. 1998. Water flow through temperate glaciers. *Reviews of Geophysics*, **36**(3), 299-328.

Gorski, M. 2004. Predominant Frequencies in the Spectrum of Ice-Vibration Events. *ACTA Geophysica Polonica*, **52**(4), 457-464.

Harrison, W.D. and A. Post. 2003. How much do we really know about glacier surging? *Annals of Glaciology*, **36**, 1-6.

Hubbard, B. and P. Nienow. 1997. Alpine Subglacial Hydrology. *Quarternary Science Reviews*, **16**, 935-969.

Iken, A., H. Rothlisberger, A. Flotron and W. Haeberli. 1983. The Uplift of Unteraargletscher at the Beginning of the Melt Season - a Consequence of Water Storage at the Bed. *Journal of Glaciology*, **29**(101), 28-47.

Iken, A. and M. Truffer. 1997. The relationship between subglacial water pressure and velocity of Findelengletscher, Switzerland, during its advance and retreat. *Journal of Glaciology*, **43**(144), 328-338.

Kamb, B., H. Engelhardt, M.A. Fahnestock, N. Humphrey, M. Meier and D. Stone. 1994. Mechanical and Hydrologic Basis for the Rapid Motion of a Large Tidewater Glacier .2. Interpretation. *Journal of Geophysical Research-Solid Earth*, **99**(B8), 15231-15244.

Kanamori, S., C.S. Benson, M. Truffer, S. Matoba, D.J. Solie and T. Shiraiwa. 2008. Seasonality of snow accumulation at Mount Wrangell, Alaska, USA. *Journal of Glaciology*, **54**(185), 273-278.

Kavanaugh, J.L. and G.K.C. Clarke. 2001. Abrupt glacier motion and reorganization of basal shear stress following the establishment of a connected drainage system. *Journal of Glaciology*, **47**(158), 472-480.

Kessler, M.A. and R.S. Anderson. 2004. Testing a numerical glacial hydrological model using spring speed-up events and outburst floods. *Geophys. Res. Lett.*, **31**.

King, R.W. and Y. Bock. 2006. Documentation for the GAMIT GPS Analysis Software. Cambridge, MA: MIT. version 10.3.

Metaxian, J.P., S. Araujo, M. Mora and P. Lesage. 2003. Seismicity related to the glacier of Cotopaxi Volcano, Ecuador. *Geophysical Research Letters*, **30**(9), 1483.

Molnia, B.F. and A. Post. 1995. Holocene History of Bering Glacier, Alaska - a Prelude to the 1993-1994 Surge. *Physical Geography*, **16**(2), 87-117.

Neave, K.G. and J.C. Savage. 1970. Icequakes on the Athabasca Glacier. *Journal of Geophysical Research*, **75**(8), 1351-1362.

Nienow, P. 1994. Dye-tracer investigations of glacier hydrological systems. (Ph.D. dissertation University of Cambridge.)

Nienow, P., M. Sharp and I. Willis. 1998. Seasonal Changes in the Morphology of the Subglacial Drainage System, Haut Glacier D'Arolla, Switzerland. *Earth Surface Processes and Landforms*, **23**, 825-843.

O'Neel, S. and W.T. Pfeffer. 2007. Source mechanics for monochromatic icequakes produced during iceberg calving at Columbia Glacier, AK. *Geophysical Research Letters*, **34**(22), L22502.

Paterson, W.S.B. 1994. *The Physics of Glaciers.* 3rd ed. Oxford, Butterworth-Heinemann (div. of Reed Ed. and Prof. Publishing Ltd).

Qamar, A. 1988. Calving Icebergs: A Source of Low-Frequency Seismic Signals From Columbia Glacier, Alaska. *Journal of Geophysical Research*, **93**(B6), 6615-6623.

Röthlisberger, H. 1972. Water Pressure in Intra- and Subglacial Channels. *Journal of Glaciology*, **11**(62), 177-203.

Röthlisberger, H. and H. Lang 1987. Glacial Hydrology. eds. Gurnell, A.M. and M.J. Clark, In *Glacio-Fluvial Sediment Transfer: An Alpine Perspective*, John Wiley and Sons, Ltd, 207-284.

Ruppert, N.A., R.A. Hansen, S. Estes, M. LaFevers, J. Sandru, G. Pavlis, M. Bauer, M. Gordon, M. Fowler and L. Lowe. 2006. Seismic component of the STEEP project, Alaska: Results of the second field season. *Eos. Trans. AGU*, 87(52). Fall Meeting Suppl. Abstract S11A-0192

Sinadinovski, C., K. Muirhead, M. Leonard, S. Spiliopoulos and D. Jepsen. 1999. Effective discrimination of icequakes on seismic records from Mawson Station. *Physics of the Earth and the Planetary Interiors*, **113**, 203-211.

Smith, A.M. 2006. Microearthquakes and subglacial conditions. *Geophysical Research Letters*, **33**(24), L24501.

St. Lawrence, W. and A. Qamar. 1979. Hydraulic Transients: A Seismic Source in Volcanoes and Glaciers. *Science*, **23**, 654-656.

Truffer, M. and W.D. Harrison. 2006. In situ measurements of till deformation and water pressure. *Journal of Glaciology*, **52**(177), 175-182.

Truffer, M., R. J. Motyka, M. Hekkers, I. M. Howat, M. A. King. In press. Terminus dynamics at an advancing glacier: Taku Glacier, Alaska. *Journal of Glaciology*.

Tsai, V.C. and G. Ekstrom. 2007. Analysis of Glacial Earthquakes. *Journal of Geophysical Research*, **112**, F03S22.

Walter, F., N. Deichmann and M. Funk. 2008. Basal icequakes during changing subglacial water pressures beneath Gornergletscher, Switzerland. *Journal of Glaciology*, **54**(186), 511-521.

Weaver, C.S. and S.D. Malone. 1979. Seismic Evidence For Discrete Glacier Motion at the Rock Ice Interface. *Journal of Glaciology*, **23**(89), 171-184.

Webb, F.H. and J.F. Zumberge. 1995. An introduction to GIPSY/OASIS-II precision software for the analysis of data from the Global Positioning System. Jet Propuls. Lab., Pasadena, CA. JPL Report D-11088, Jul. 17–21, 1995.

Wiens, D.A., S. Anandakrishnan, J.P. Winberry and M.A. King. 2008. Simultaneous teleseismic and geodetic observations of the stick-slip motion of an Antarctic ice stream. *Nature*, **453**(7196), 770-U3.

Willis, I.C. 1995. Interannual Variations in Glacier Motion - a Review. *Progress in Physical Geography*, **19**(1), 61-106.

Wolf, L. and J. Davies. 1986. Glacier-Generated Earthquakes from Prince William Sound, Alaska. *Bulletin of the Seismological Society of America*, **76**(2), 367-379.

APPENDIX A

Supplementary Figures

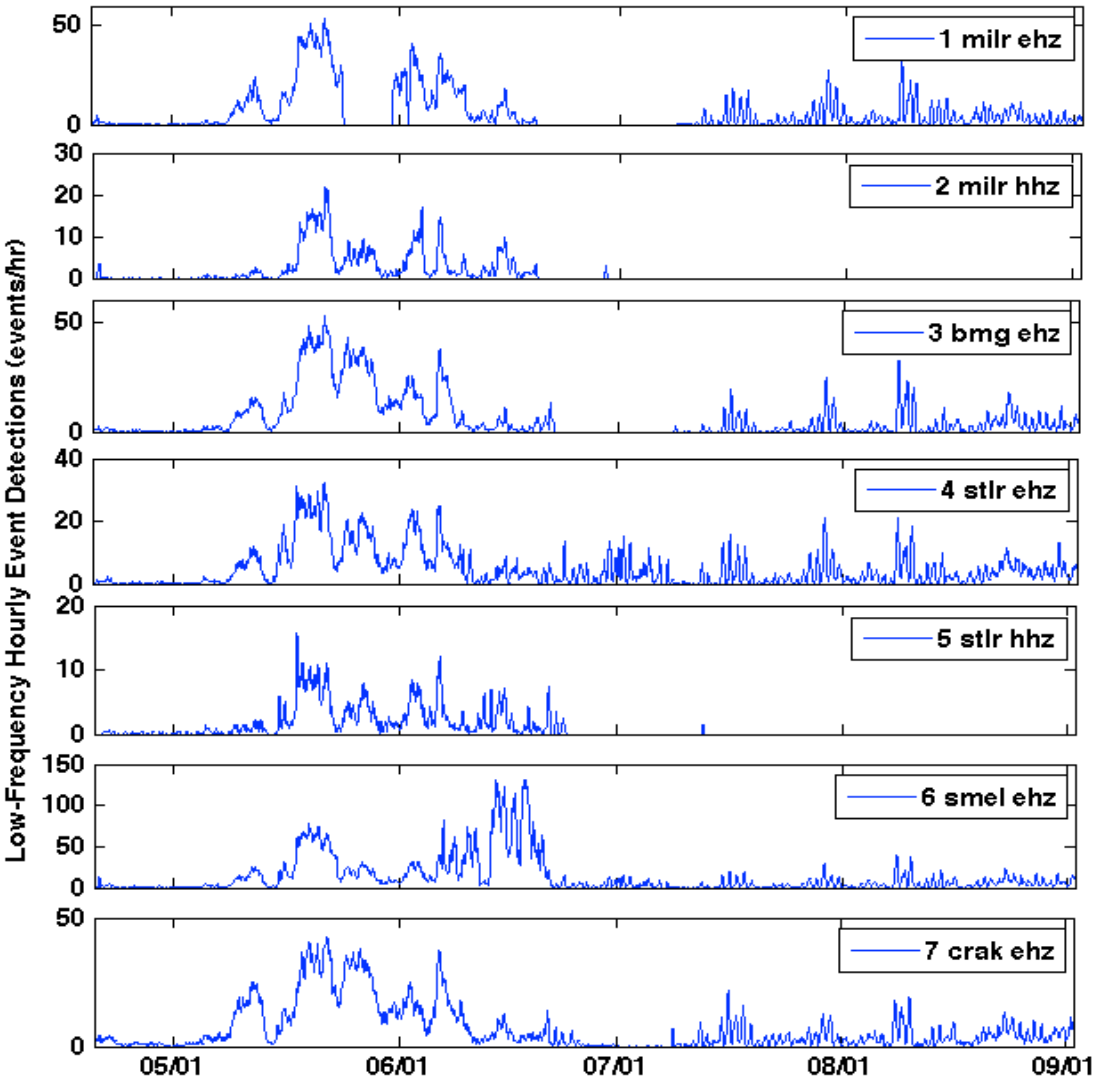

Figure 1. Low-Frequency Hourly Event Detections. To demonstrate the variations from station to station in detection levels, we have plotted the LF hourly event detections for each (the HF detections show similar variations between stations). During the first month and a half of the study, we also had broadband seismometers. These are not included in the analysis, but have been plotted here for historical reference. 'EHZ' is the vertical channel of the L22 short period seismometers and 'HHZ' is the vertical channel of the 6TD broadband seismometers.

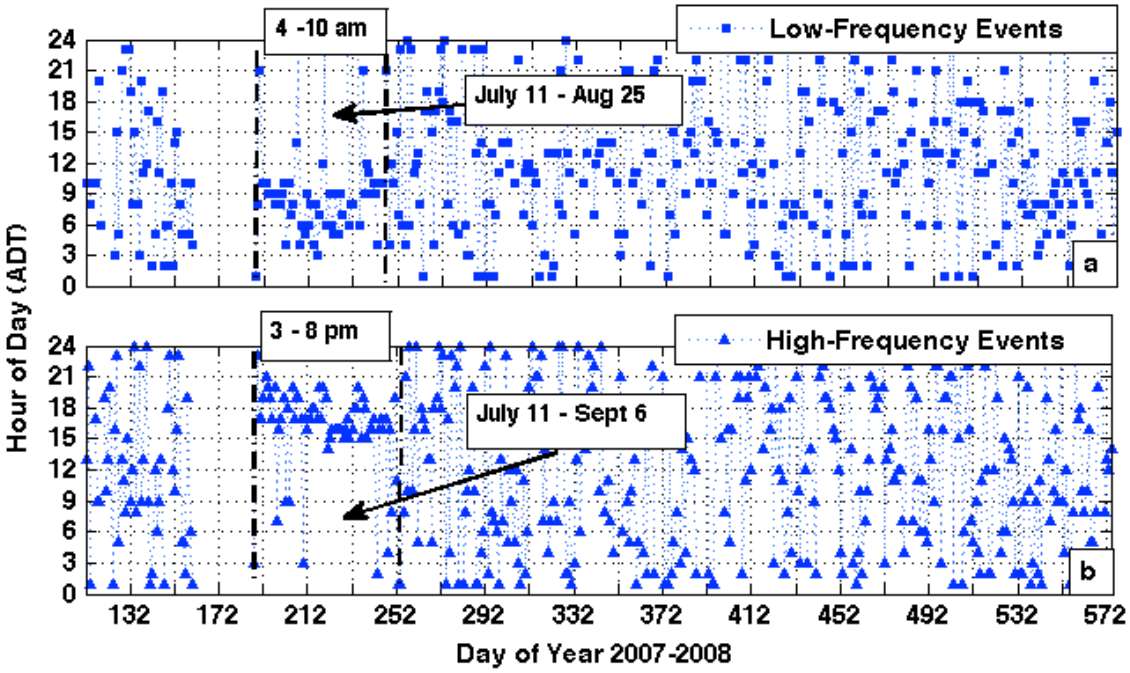

Figure 2. Hour of Day of Daily Maximum Icequake Occurrence. The hourly event count shows no preference to daily time of maximum occurrence, except during the summer months. The difference in timing of the LF (a) and HF (b) events supports that they are generated by different source mechanisms.

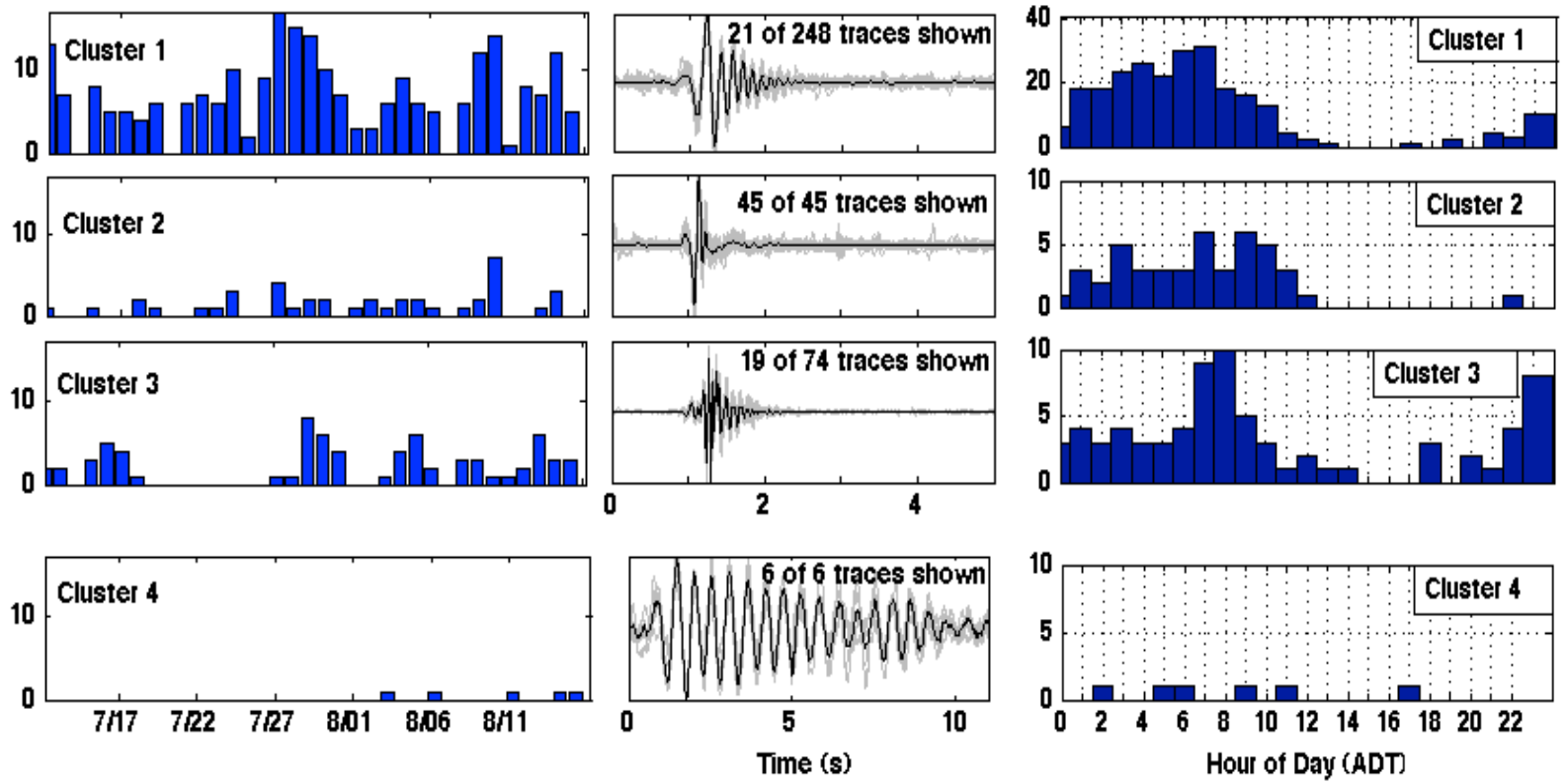

Figure 3. Mid-Summer Repeating Events of 2007. The left column shows the number of events occurring per day. The middle column shows the waveforms of each cluster. The light gray lines are the individual waveforms and the black line is a stack of all the waveforms. The right column shows the number of events that occur for each hour of the day over the period from 7/12/2007 to 8/16/2007.

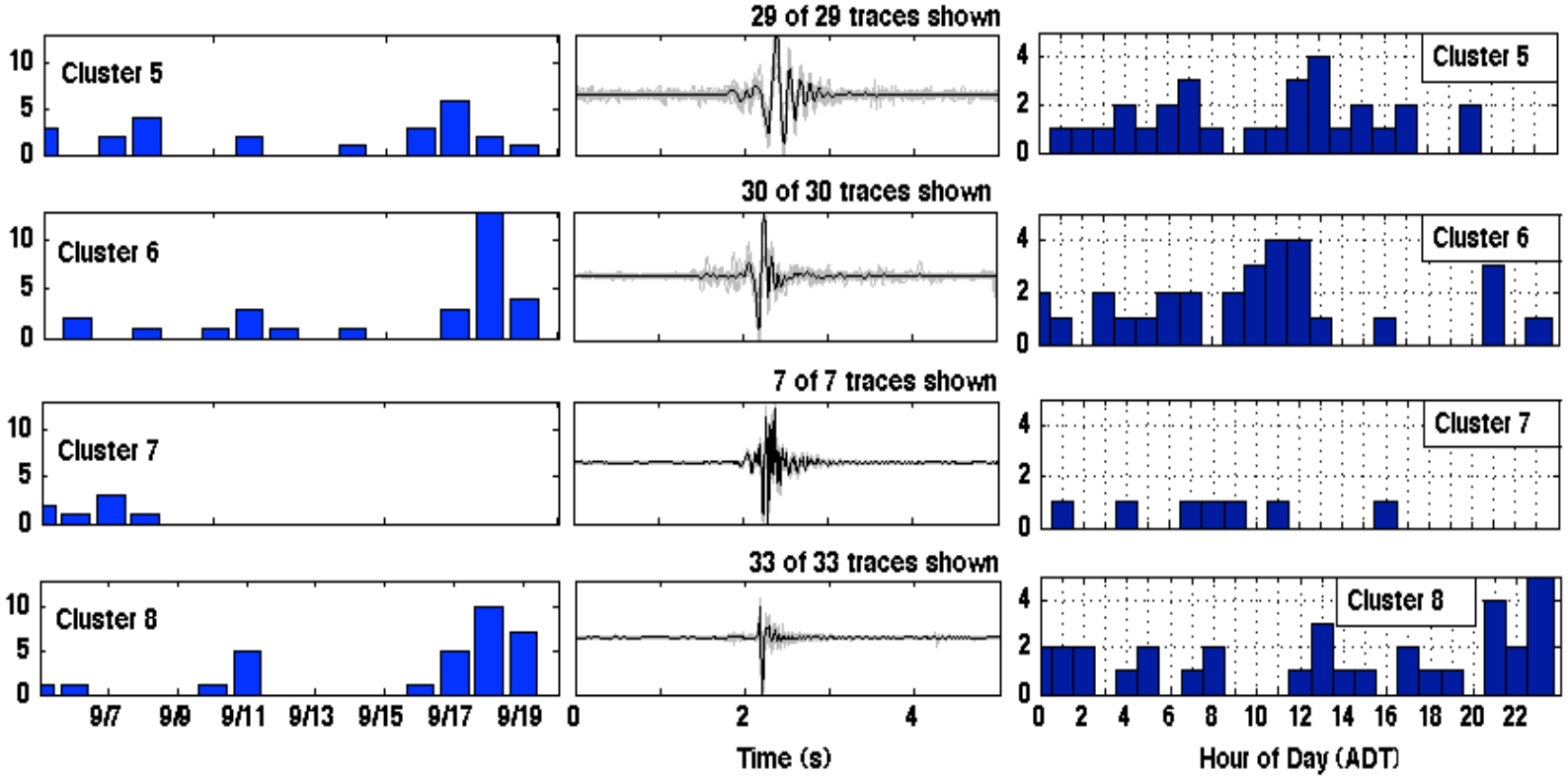

Figure 4. September Repeating Events of 2007. The left column shows the number of events occurring per day. The middle column shows the waveforms of each cluster. The light gray lines are the individual waveforms and the black line is a stack of all the waveforms. The right column shows the number of events that occur for each hour of the day over the period from 9/5/2007 to 9/20/2007.

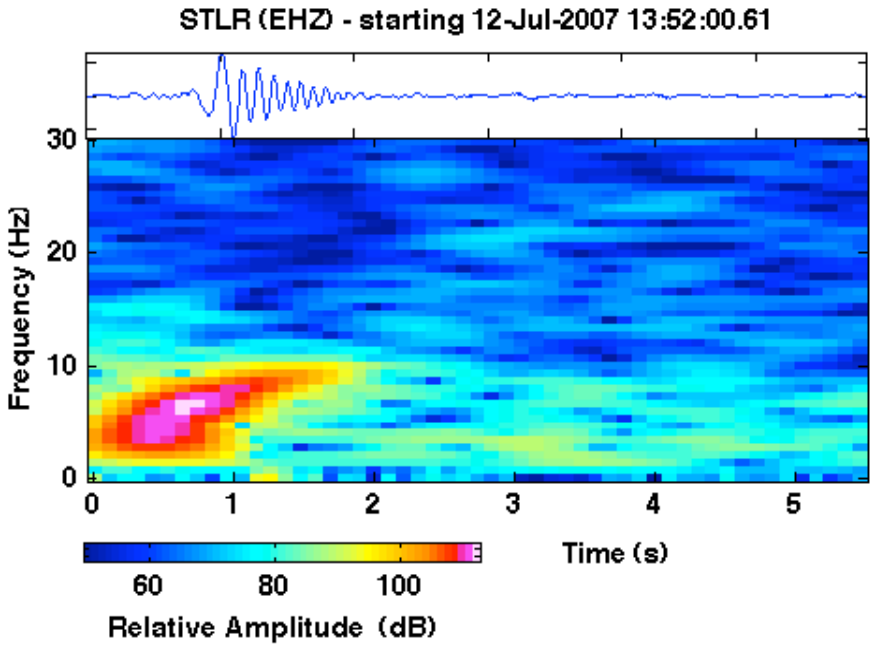

Figure 5. Spectogram of a waveform from Cluster 1. Events of this group have dominant frequencies of 3-7 Hz and a frequency range of 2-15 Hz. At top of figure is the station, channel, and trigger time.

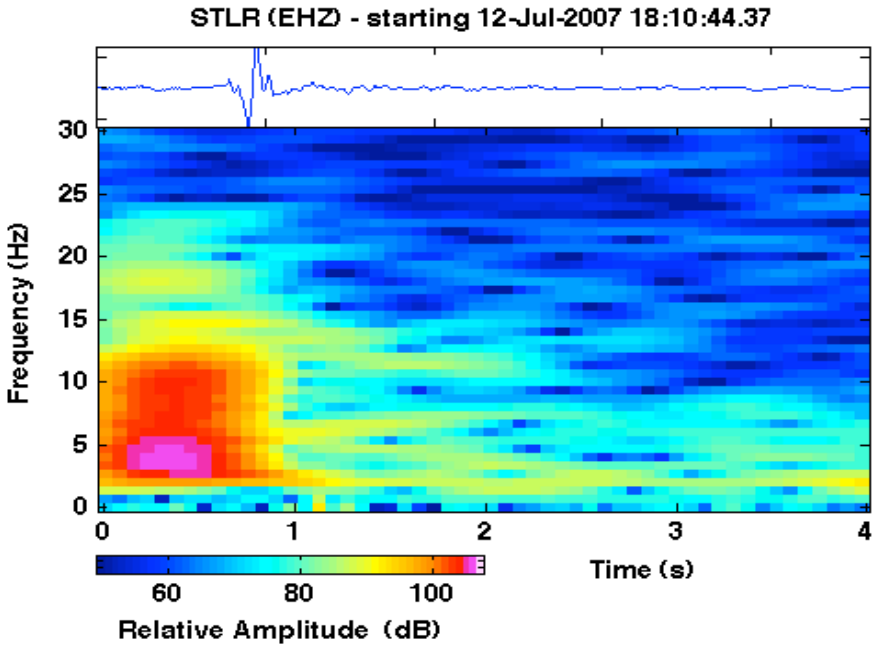

Figure 6. Spectogram of a waveform from Cluster 2. Events of this group have dominant frequencies of 3-7 Hz and a frequency range of 2-25 Hz. At top of figure is the station, channel, and trigger time.

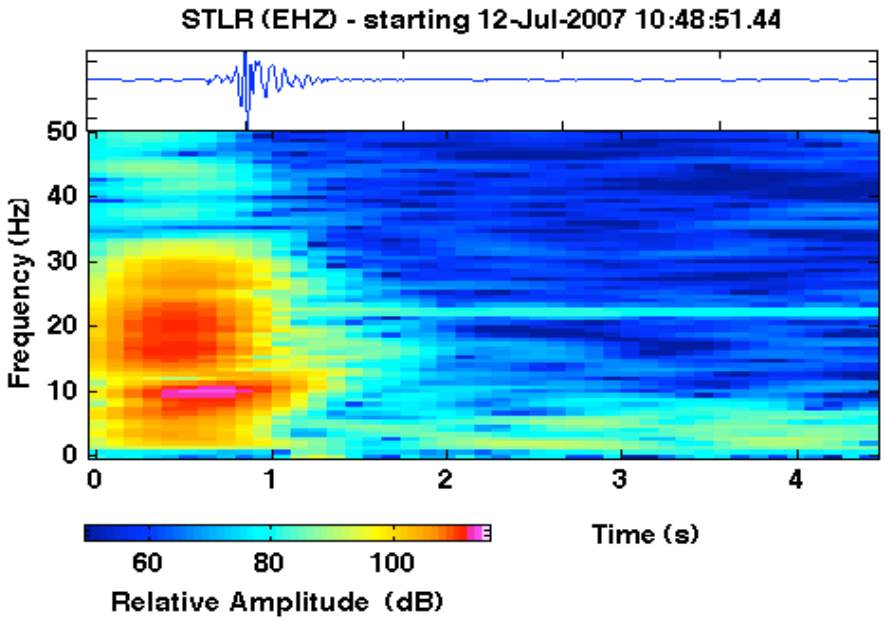

Figure 7. Spectogram of a waveform from Cluster 3. Events of this group have dominant frequencies of 8 & 20 Hz and a frequency range of 2-40 Hz. At top of figure is the station, channel, and trigger time.

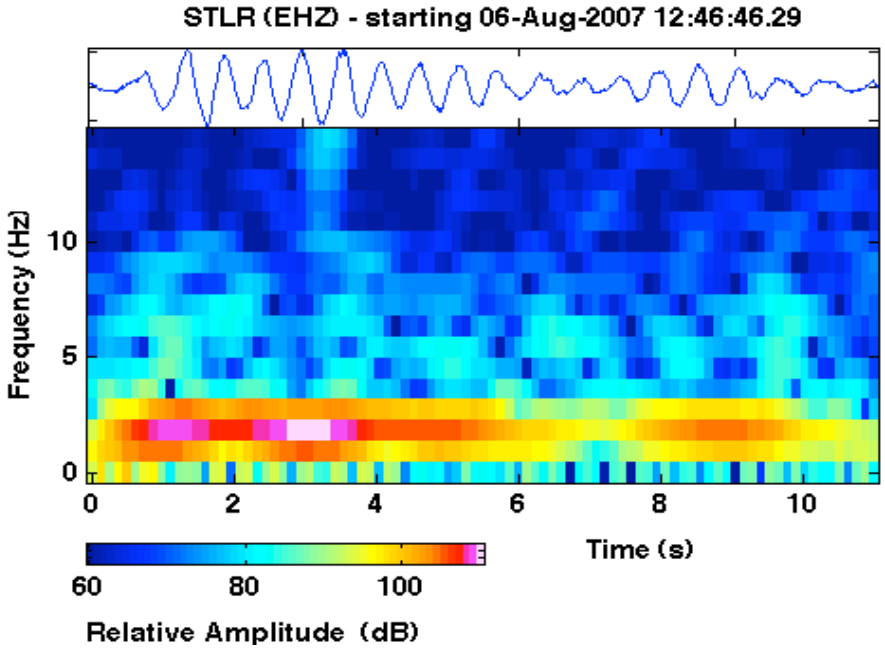

Figure 8. Spectogram of a waveform from Cluster 4. Events of this group have dominant frequencies of 2 Hz and a frequency range of 1-7 Hz. At top of figure is the station, channel, and trigger time.

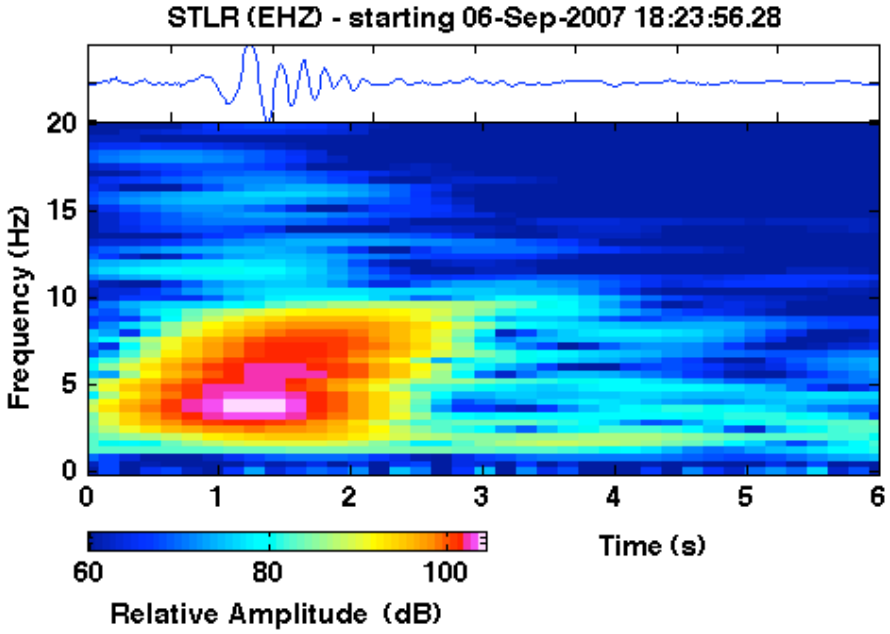

Figure 9. Spectogram of a waveform from Cluster 5. Events of this group have dominant frequencies of 5 Hz and a frequency range of 2-12 Hz. At top of figure is the station, channel, and trigger time.

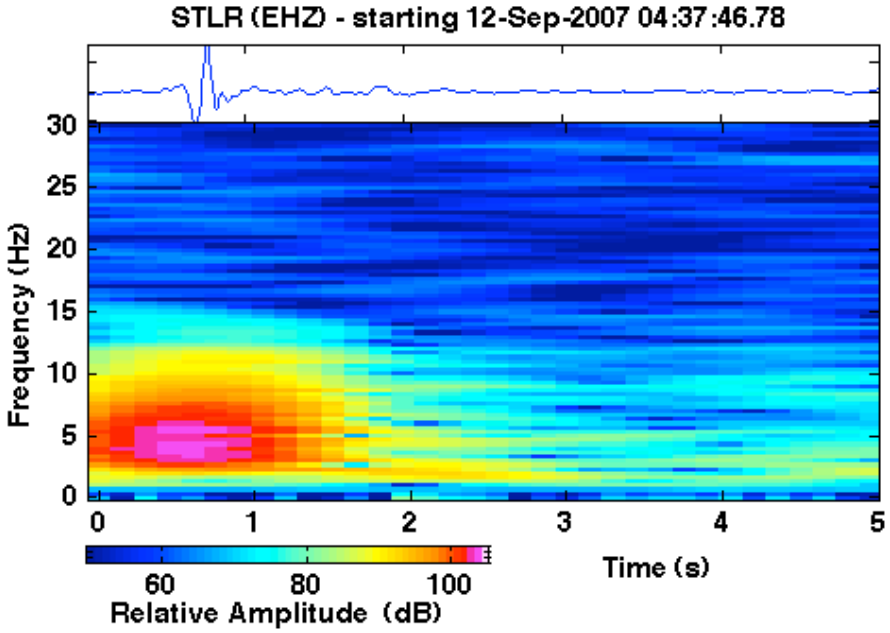

Figure 10. Spectogram of a waveform from Cluster 6. Events of this group have dominant frequencies of 6 Hz and a frequency range of 2-15 Hz. At top of figure is the station, channel, and trigger time.

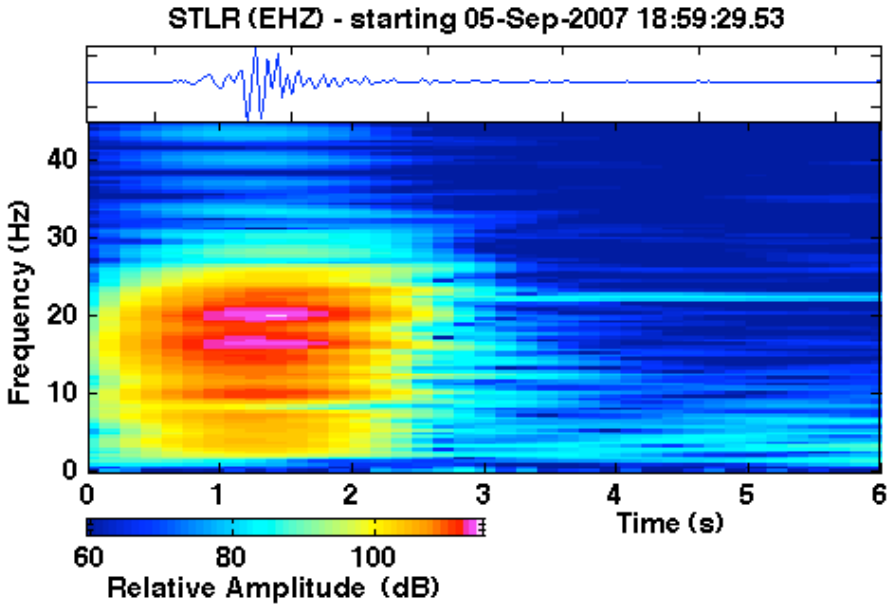

Figure 11. Spectogram of a waveform from Cluster 7. Events of this group have dominant frequencies of 9 & 20 Hz and a frequency range of 2-30 Hz. At top of figure is the station, channel, and trigger time.

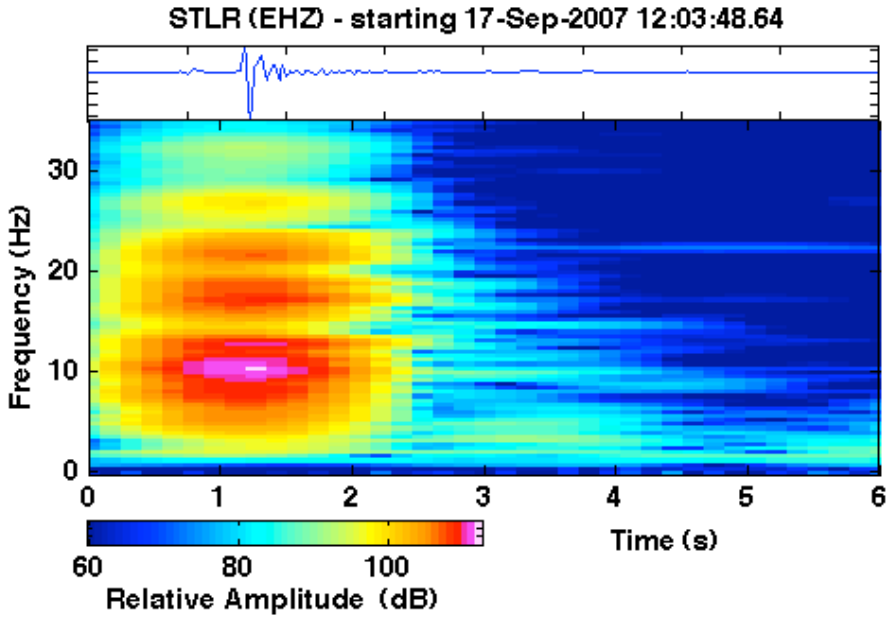

Figure 12. Spectogram of a waveform from Cluster 7. Events of this group have dominant frequencies of 8-10 & 15-17 Hz and a frequency range of 2-40 Hz. At top of figure is the station, channel, and trigger time.

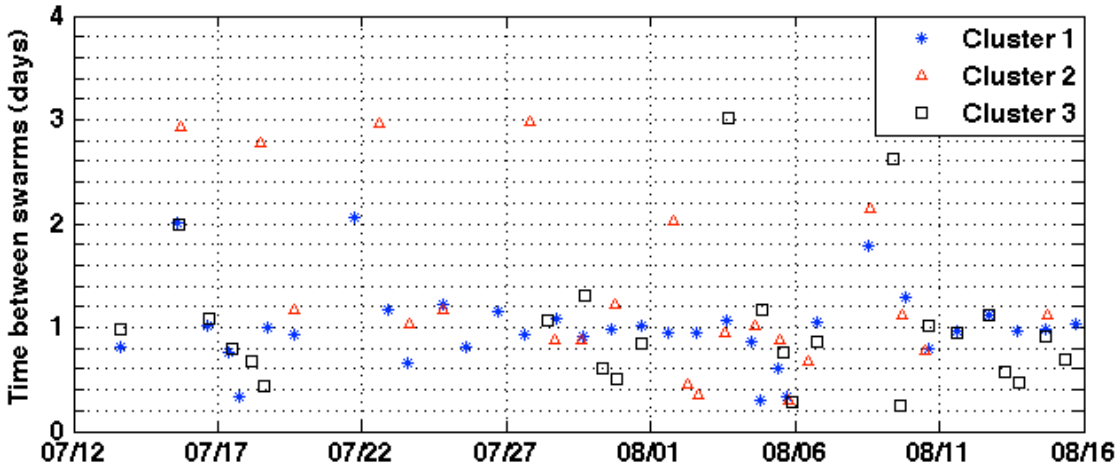

Figure 13. Diurnal Signal of Clusters 1-3 as demonstrated by the timing between event swarms. First, the elapsed time between trigger times was calculated. Any events that happened successively with less than 6 hrs between their arrivals were grouped into 'event swarms'. The time between event swarms was calculated and is shown here. This plot shows that event swarms occur with a roughly diurnal frequency (especially with Cluster 1).

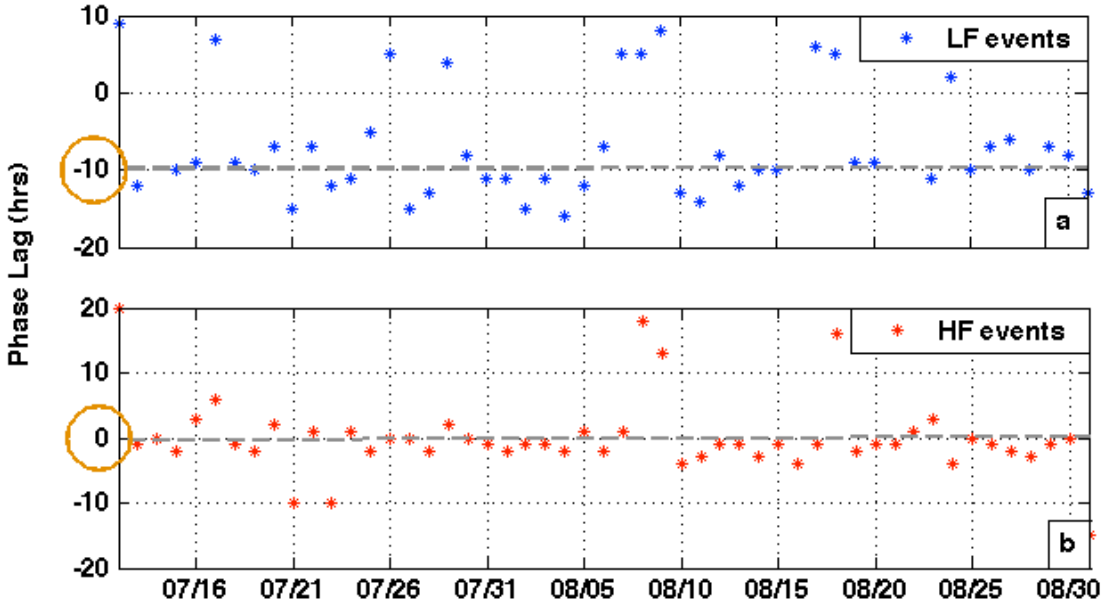

Figure 14. The phase lag between maximums in icequake occurrence and ice velocity. Class 1 events generally lag the velocity by ~10 hours and are roughly out of phase. Class 3 events are generally in-phase with velocity, showing only several hours of phase difference.

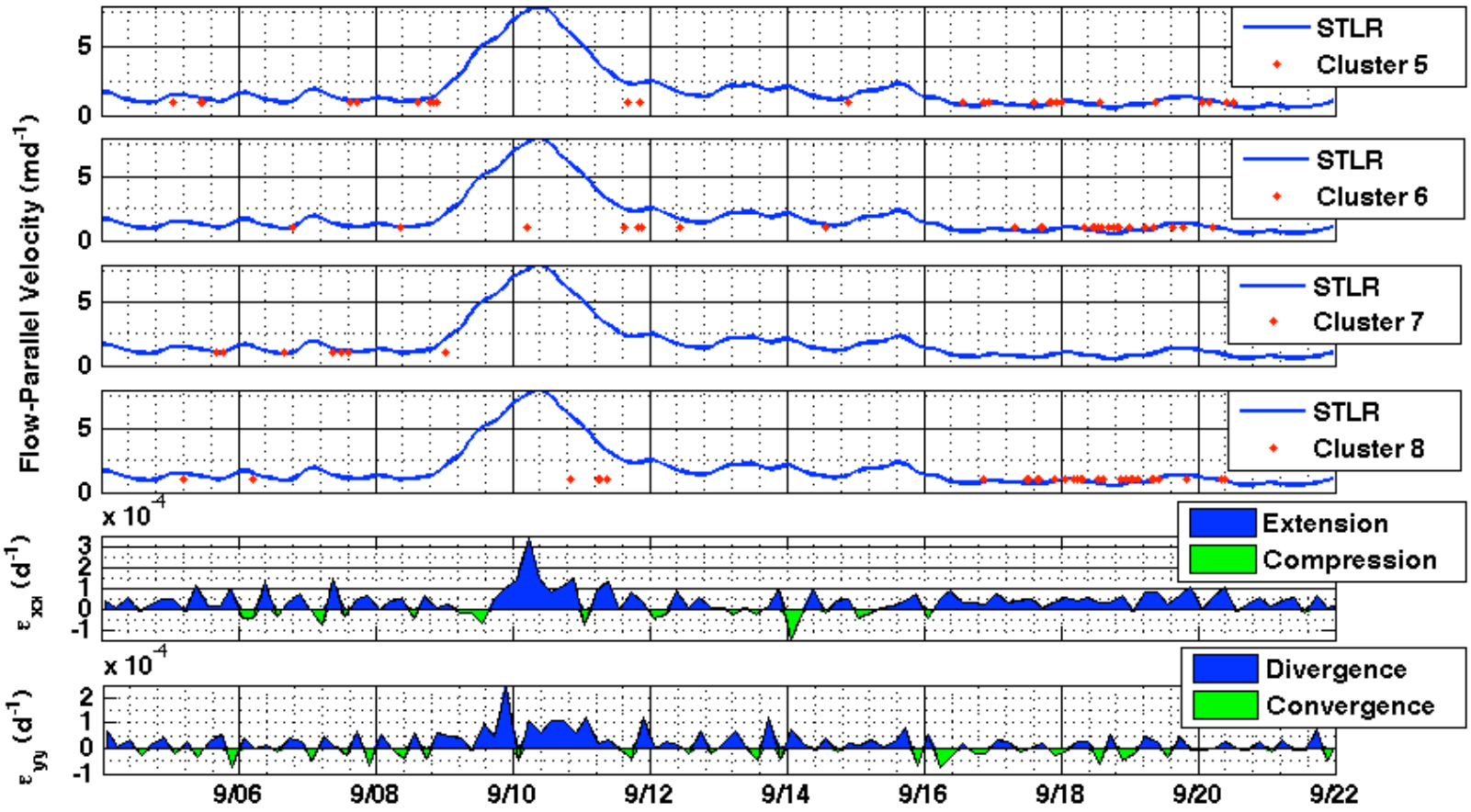

Figure 15. September comparison of the timing of repeating events and ice motion. The first four plots show horizontal velocity compared with the trigger times of Clusters 5-8. The last two plots show the longitudinal (ε_{xx}) and transverse (ε_{yy}) strain rates. The blue and green coloring identifies positive and negative strain rates. Clusters 6 and 8 show a significant increase after 9/16. Cluster 7 does not occur after 9/9.

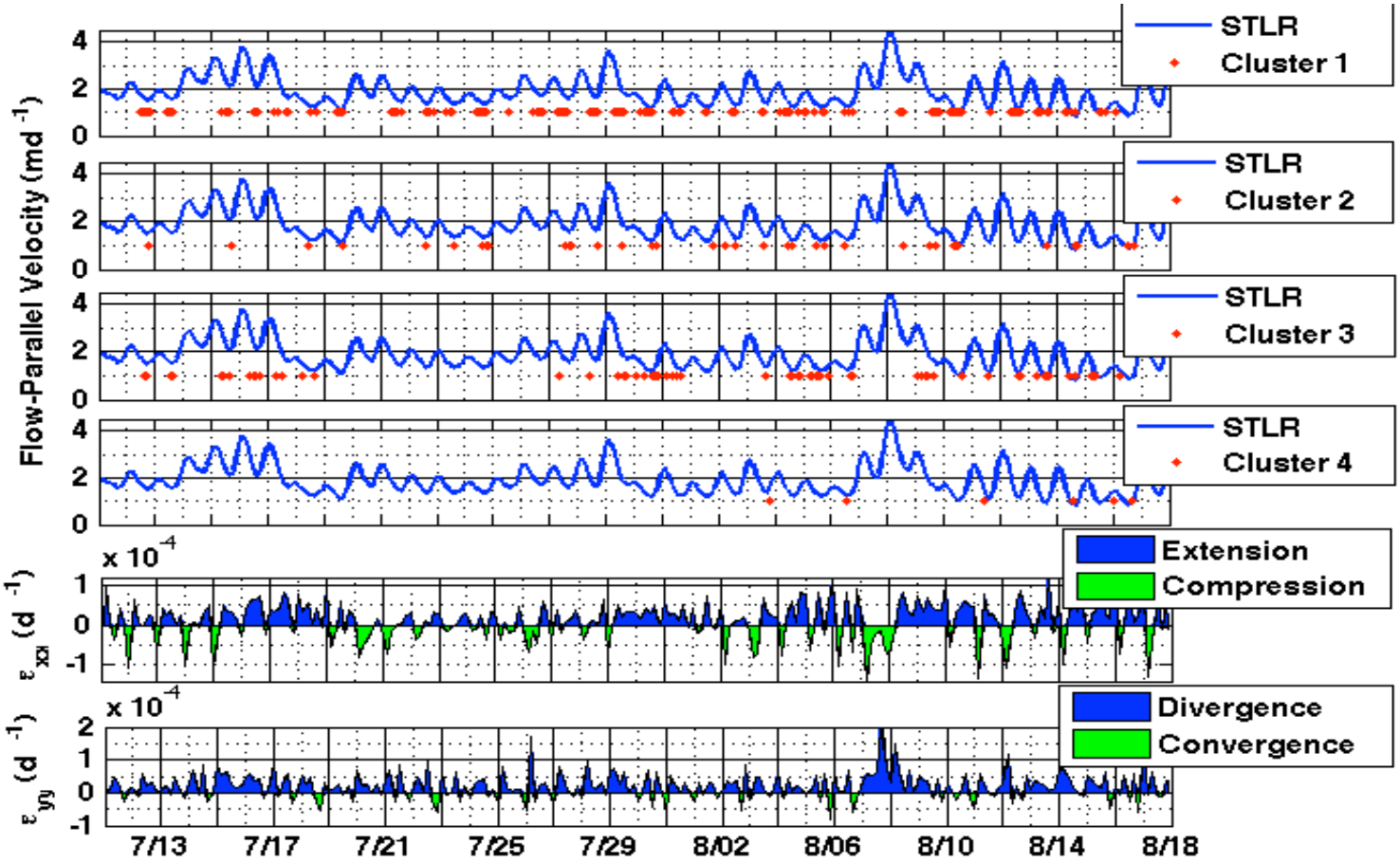

Figure 16. Mid-summer comparison of the timing of repeating events and ice motion. The first four plots show horizontal velocity compared with the trigger times of Clusters 1-4. The last two plots show the longitudinal (ε_{xx}) and transverse (ε_{yy}) strain rates. The blue and green coloring identifies positive and negative strain rates. Most of the cluster events occur during decreasing or minimum velocities and with extensional strain rates.

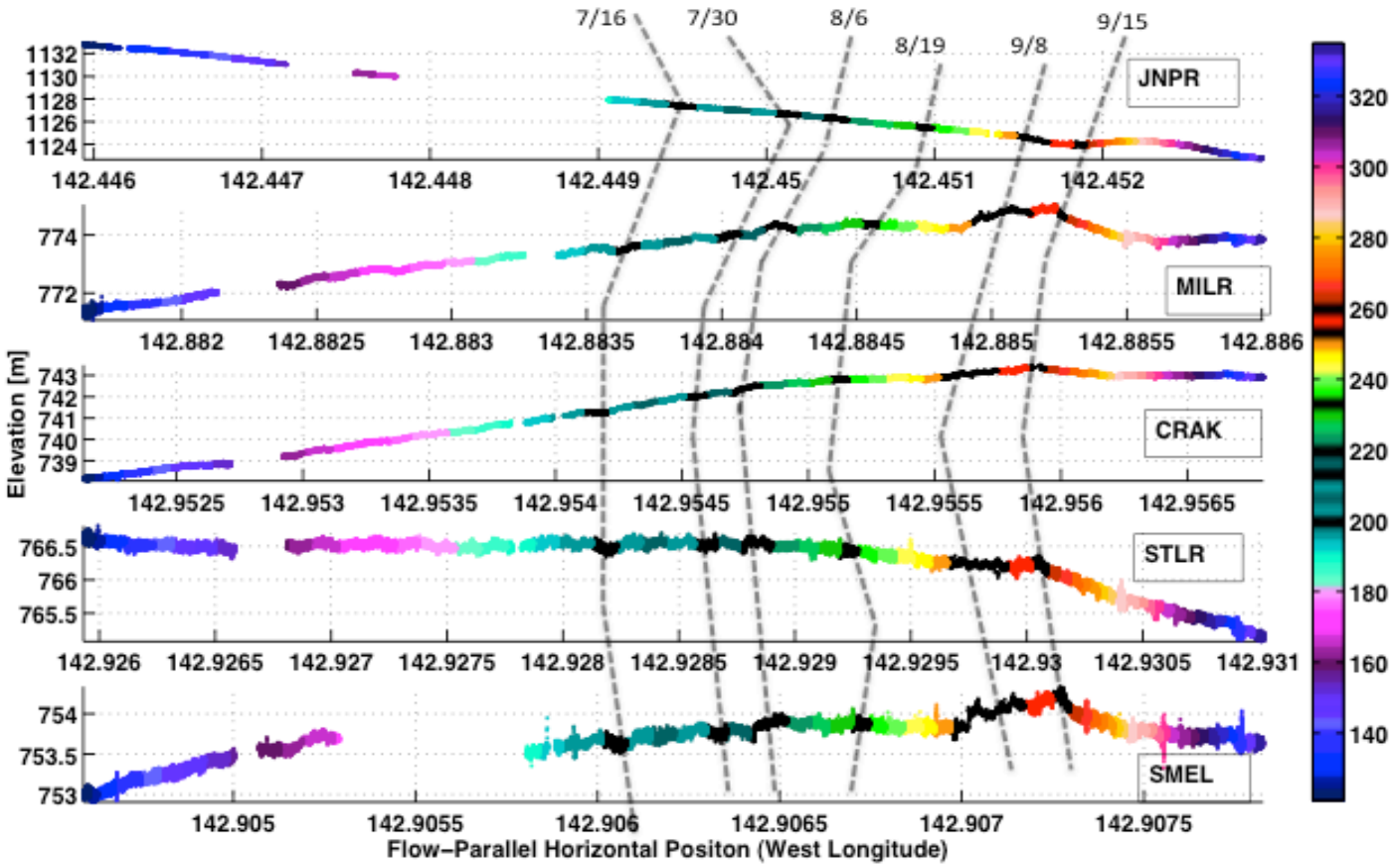

Figure 16. Vertical Displacement plotted against horizontal position (5-minute positions). The time (in day of year) is represented by the colorbar. Dashed lines identify days with notable vertical motion (or shifts in motion trends).

APPENDIX B

Detection Parameter File to be used with Antelope Environmental Data Collection Software (Boulder Real Time Technologies: http://www.brtt.com/software.html)

Designed (by Mike West, GI Seismology) and used to detect three classes of icequakes within the Bering data

```
# CUSTOM PARAMETER FILE FOR DBDETECT

##########################################################################

# DEFAULTS (MOSTLY OVERWRITTEN BELOW)

ave_type        rms     # Method for averaging (rms or filter)
sta_twin        0.5     # short term average time window
sta_tmin        0.5     # short term average minimum time for average
sta_maxtgap     0.5     # short term average maximum time gap
lta_twin        8.0# long term average time window
lta_tmin        4.0     # long term average minimum time for average
lta_maxtgap     4.0     # long term average maximum time gap
nodet_twin      0.0     # no detection if on time is less than this ###-MEW
pamp            500.0   # plot amplitude
thresh          5.0     # detection SNR threshold
threshoff       2.5     # detection-off SNR threshold
det_tmin        0.5     # detection minimum on time ###-MEW
det_tmax        10.0    # detection maximum on time
h               0       # plot channel height in pixels
filter          none    # default filter
iphase          P       # default iphase for detections
process_twin    3600.0  # data is processed in hunks of this duration

##########################################################################

# NOTES ON SETTINGS

#   sta_tmin: default pf sets a" sta_tmin = sta_twin
#   sta_maxtgap: default pf have 0.5 for all 1/2*sta_tmin seems appropriate
#   lta_twin: at least 5 times sta_twin
#   lta_tmin: default pf has lta_tmin = 1/2 * lta_twin
#   lta_maxtgap: seems appropriate to set it to 1/2*lta_twin
#   filter: sta_twin should be >1.6 times the the low filter *period*

##########################################################################

# BAND AVO MIMICS AVO EARTHWORM DETECTIONS
```

```
#       - HF detector
#       - LF detector
#       - Crevassing detector
bands   &Tbl{
        &Arr{
                sta_twin        0.5
                sta_tmin        0.5
                sta_maxtgap     0.5
                lta_twin        8.0
                lta_tmin        4.0
                lta_maxtgap     4.0
                nodet_twin      0.0
                thresh          5
                threshoff       2.5
                filter          BW 3.0 4 20 4
#       }

#       &Arr{
                sta_twin        2.0
                sta_tmin        2.0
                sta_maxtgap     0.5
                lta_twin        10.0
                lta_tmin        5.0
                lta_maxtgap     5.0
                thresh          5
                threshoff       2.5
                filter          BW 0.8 4 5 4
#       }

#       &Arr{
                sta_twin        0.2
                sta_tmin        0.2
                sta_maxtgap     0.5
                lta_twin        2.0
                lta_tmin        1.0
                lta_maxtgap     1.0
                thresh          5
                threshoff       2.5
                filter          BW 8 4 50 4
#       }

}

##############################################################################
# STATIONS AND CHANNELS

# format: sta_term    chan_term
stachans        &Tbl{
```

```
        MILR   .HZ
        STLR   .HZ
        BMG    .HZ
        CRAK   .HZ
        SMEL   .HZ
}

# Individual channels may be rejected or ovewritten. See man page for details

#       channels to reject

reject &Tbl{
}
```